THE ASTROPHYSICAL JOURNAL, 556:601–618, 2001 August 1

MASS AND LIGHT IN THE UNIVERSE[1]

GILLIAN WILSON,[2,3] NICK KAISER,[2] AND GERARD A. LUPPINO[2]

Received 2000 September 20; accepted 2001 February 12

ABSTRACT

We present a weak lensing and photometric study of six $0.^{\circ}5 \times 0.^{\circ}5$ fields observed at the Canada-France-Hawaii Telescope using the UH8K CCD mosaic camera. The fields were observed for a total of 2 hr each in I and V, resulting in catalogs containing $\sim$20,000 galaxies per passband per field. We use $V-I$ color and I magnitude to select bright early-type galaxies at redshifts $0.1 < z < 0.9$. We measure the gravitational shear from faint galaxies in the range $21 < m_I < 25$ from a composite catalog and find a strong correlation with that predicted from the early types if they trace the mass with $M/L_B \simeq 300 \pm 75\ h\ M_{\odot}/L_{\odot}$ for a flat ($\Omega_{m0} = 0.3$, $\Omega_{\lambda 0} = 0.7$) lambda cosmology and $M/L_B \simeq 400 \pm 100\ h\ M_{\odot}/L_{\odot}$ for Einstein–de Sitter. We make two-dimensional reconstructions of the mass surface density. Cross-correlation of the measured mass surface density with that predicted from the early-type galaxy distribution shows a strong peak at zero lag (significant at the 5.2 σ level). We azimuthally average the cross-correlation and autocorrelation functions. We conclude that the profiles are consistent with early-type galaxies tracing mass on scales of $\geq 45''$ ($\geq 200\ h^{-1}$ kpc at $z = 0.5$). We subdivide our bright early-type galaxies by redshift and obtain similar conclusions. These M/L_B ratios imply $\Omega_{m0} \simeq 0.10 \pm 0.02$ ($\Omega_{m0} \simeq 0.13 \pm 0.03$ for Einstein–de Sitter) of closure density.

Subject headings: cosmology: observations — dark matter — galaxies: evolution — galaxies: photometry — gravitational lensing — large-scale structure of universe

1. INTRODUCTION

It is well known that a large quantity of dark matter exists in the universe. Evidence for dark matter around luminous galaxies comes from stellar velocity dispersions and rotation curves in the outer parts of spiral galaxies (Faber & Gallagher 1979; Bosma 1981; Trimble 1987) and large velocity dispersions (Faber & Gallagher 1979; Trimble 1987) and extended X-ray halos of hot gas (Mushotzky et al. 1994; Trinchieri et al. 1994; Kim & Fabbiano 1995; Trinchieri, Fabbiano, & Kim 1997) in elliptical galaxies. On larger scales, evidence for dark matter in clusters comes from gravitational lensing (Mellier 1999, and references therein), virial analyses (Carlberg et al. 1996), or X-ray halos of hot gas (White & Fabian 1995). Evidence for dark matter in the field comes from relative motions of galaxies in the Local Group (Turner 1976; Sandage 1986; Jing, Mo, & Boerner 1998), or relative motions of faint satellites (Bahcall & Tremaine 1981; Zaritsky et al. 1997), or pairs of galaxies analyzed statistically (Turner 1976; Brown & Peebles 1987; Davis, Miller, & White 1997; Jing et al. 1998). On still larger scales of 0.25–3 h^{-1} Mpc, evidence for dark matter comes from the cosmic virial theorem analysis (Davis & Peebles 1983) and least-action method (Shaya, Peebles, & Tully 1995), and on 10–30 h^{-1} Mpc scales, from bulk flows and redshift-space anisotropies (Strauss & Willick 1995 and references therein).

The relative contribution of the dark-matter component is usually specified in terms of the mass-to-light ratio, M/L, the ratio of the total mass relative to the total light within a given scale. It is generally acknowledged that the M/L ratio increases from the bright luminous regions of galaxies to their faint halos, with possible further increase on larger scale to systems such as groups and rich clusters of galaxies. The first measurement of the M/L ratio in the Coma Cluster (Zwicky 1933) obtained $M/L \sim 300\ h\ M_{\odot}/L_{\odot}$. Subsequent measurements of a series of clusters have confirmed his original numbers (Carlberg, Yee, & Ellingson 1997 find a virial $M/L = 213 \pm 59$ for galaxy clusters assuming an $\Omega_{m0} = 0.2$, $\Omega_{\lambda 0} = 0.0$ cosmology—see also Carlberg et al. 1996). If the Coma M/L ratio is universal, then the density parameter of the universe would appear to be $\Omega_{m0} \simeq 0.2$. If one wished to reconcile cluster M/L ratios with the philosophically appealing value of $\Omega_{m0} = 1$, one was forced to argue that the efficiency of galaxy formation must therefore be biased (enhanced) in dense environments (Kaiser 1984; Bardeen et al. 1986). As one measured M/L on larger and larger scales, one might expect the M/L ratio to increase until one approached the true global value of $\Omega_{m0} = 1$. Motivated by such reasoning, much effort has been expended, both in simulating bias on galaxy, cluster, or large-scale structure scales (Davis et al. 1985) and also in attempting to measure its presence from large-scale galaxy bulk flows (Sigad et al. 1998; Willick & Strauss 1998; Branchini et al. 2000). For a time, the idea that M/L ratios increased as a function of increasing scale seemed very plausible. A very clear summary of M/L ratio with scale from a variety of methods is given in Bahcall, Lubin, & Dorman (1995, hereafter BLD). In that paper, however, it is argued that while M/L increases with scale to $\simeq 200\ h^{-1}$ kpc, there is little evidence that M/L ratios increase on scales beyond that. BLD argued that the total mass of large-scale systems such as groups, rich clusters, and superclusters could be accounted for by the total mass of their member galaxies, including their large halos and intracluster gas. They argued for $M/L_B \simeq 100\ h\ M_{\odot}/L_{\odot}$ for late-type galaxies and $M/L_B \simeq 400\ h\ M_{\odot}/L_{\odot}$ for early-type galaxies and concluded that these values implied $\Omega_{m0} \sim 0.2$–0.3.

[1] Based on observations with the Canada-France-Hawaii Telescope, which is operated by the National Research Council of Canada, le Centre National de la Recherche Scientifique de France, and the University of Hawaii.

[2] Institute for Astronomy, University of Hawaii, 2680 Woodlawn Drive, Honolulu, HI 96822.

[3] Physics Department, Brown University, 182 Hope Street, Providence, RI 02912; gillian@het.brown.edu.

TABLE 1

FIELD CENTERS AND SEEING

Field	Pointing	R.A. (J2000)	Decl. (J2000)	l	b	FWHM (I) (arcsec)	FWHM (V) (arcsec)
Lockman.....	1	10 52 43.0	57 28 48.0	149.28	53.15	0.83	0.85
	2	10 56 43.0	58 28 48.0	147.47	52.83	0.84	0.86
Groth	1	14 16 46.0	52 30 12.0	96.60	60.04	0.80	0.93
	3	14 09 00.0	51 30 00.0	97.19	61.57	0.70	0.85
1650	1	16 51 49.0	34 55 02.0	57.37	38.67	0.82	0.85
	3	16 56 00.0	35 45 00.0	58.58	37.95	0.85	0.72

NOTE.—Units of right ascension are hours, minutes, and seconds, and units of declination are degrees, arcminutes, and arcseconds.

Strong evidence from Kaiser et al. (2001c, hereafter KWLK) also suggested a similar picture. In that paper, "A Photometric and Weak Lensing Analysis of the $z = 0.42$ Supercluster MS0302+17," it was shown on scales ≥ 200 h^{-1} kpc that *early*-type galaxy light traces mass with $M/L_B \simeq 250 \pm 50\ h\ M_\odot/L_\odot$. This was the first time that mass had been measured out to such a large radial distance ($\simeq 3\ h^{-1}$ Mpc) from a cluster center using such a "direct" technique as gravitational lensing. This "light-traces-mass" relationship was somewhat surprising and intriguing. It raised the question of whether the relationship (and indeed M/L_B value) was applicable exclusively to early-type galaxies in rich cluster environments or was applicable to early-type galaxies in all environments in the universe.

This paper investigates the relationship between mass and luminosity on scales of up to 30′ using data collected at the Canada-France-Hawaii Telescope (CFHT) with the UH8K camera. Our analysis differs from previous lensing studies in that here we focus on "blank fields," i.e., the fields chosen for study were intended to be representative views of the universe not containing any unusually large masses such as rich clusters. We investigate the same hypothesis as proposed in KWLK—namely, that early-type galaxy light traces mass with a constant ratio of proportionality.

The outline of the paper is as follows. In § 2 we describe the data and the selection of lens and background galaxies. We also present surface mass density reconstructions from shear estimates. In § 3 we compare these to predictions inferred from the luminosity of early-type galaxies at various redshifts. In § 4 we discuss our results. We calculate the mean mass-to-light ratio of an early-type galaxy and the contribution of early types to the closure density. We investigate the dependence of these values on cosmology. We then compare our values of M/L_B and Ω_{m0} with other studies. We also consider possible sources of uncertainty. In § 5 we briefly summarize our conclusions. We assume a flat lambda ($\Omega_{m0} = 0.3$, $\Omega_{\lambda 0} = 0.7$) cosmology with $H_0 = 100\ h$ km s^{-1} Mpc^{-1} throughout unless explicitly stated otherwise.

TABLE 2

LENS GALAXY DATA

Lens Redshift	Number Lens	$\Sigma_{\rm crit}^{-1}$ ($\times 10^{-16}\ h^{-1}$ Mpc^2 $M_\odot^{-1}$)[a]
0.1 ± 0.05.....	92	1.36
0.2 ± 0.05.....	222	2.04
0.3 ± 0.05.....	366	2.28
0.4 ± 0.05.....	960	2.26
0.5 ± 0.05.....	1611	2.10
0.6 ± 0.05.....	663	1.86
0.7 ± 0.05.....	699	1.61
0.8 ± 0.05.....	594	1.36
0.9 ± 0.05.....	233	1.13

[a] Cosmology dependent ($\Omega_{\rm m0} = 0.3$, $\Omega_{\lambda 0} = 0.7$ assumed here).

2. THE DATA AND GALAXY SAMPLES

2.1. *Data Acquisition and Reduction*

The data were taken at the 3.6 m CFHT telescope using the 8192 × 8192 pixel UH8K camera at prime focus. The field of view of this camera is $\simeq 30'$ with pixel size $\simeq 0\farcs207$. The data (six pointings) used in the analysis were acquired as part of an ongoing project, the principle aim of which is to investigate the cosmic shear pattern caused by gravitational lensing from the large-scale structure of the universe. Table 1 gives an overview of the data, describing the field name, center, and seeing for each pointing. This is the third in a series of papers describing results from the large-scale structure project. Kaiser, Wilson, & Luppino (2001a, hereafter Paper I) presented estimates of cosmic shear variance on 2′–30′ scales, and Wilson et al. (2001, hereafter Paper II) investigated galaxy halos at radii of 20″–60″ (50–200 h^{-1} kpc). Here we focus on mass and light on galaxy group and cluster scales. A forthcoming paper will address galaxy clustering. Further details of the data reduction pipeline may be found in Kaiser et al. (2001b) and, as already mentioned in the Introduction, an application to the ms0302 supercluster in KWLK. In brief, the data were dark-subtracted, flat-fielded, registered, median-averaged, and corrected for galactic extinction. A full description of our catalogs will be presented in a later paper (G. Wilson & N. Kaiser 2001, in preparation).

2.2. *Lens Galaxy Sample*

Our analysis differs from other approaches in that we use $V-I$ color to select a sample of bright early-type lens galaxies with reasonably well-determined redshifts. As we will

TABLE 3

GALAXY CATALOGS

Field	Pointing	I	V	IV
Lockman.....	1	20820	20358	25963
	2	20428	17782	23835
Groth	1	27906	16391	29437
	3	19300	15876	22989
1650	1	21785	15403	24494
	3	18391	16518	22894

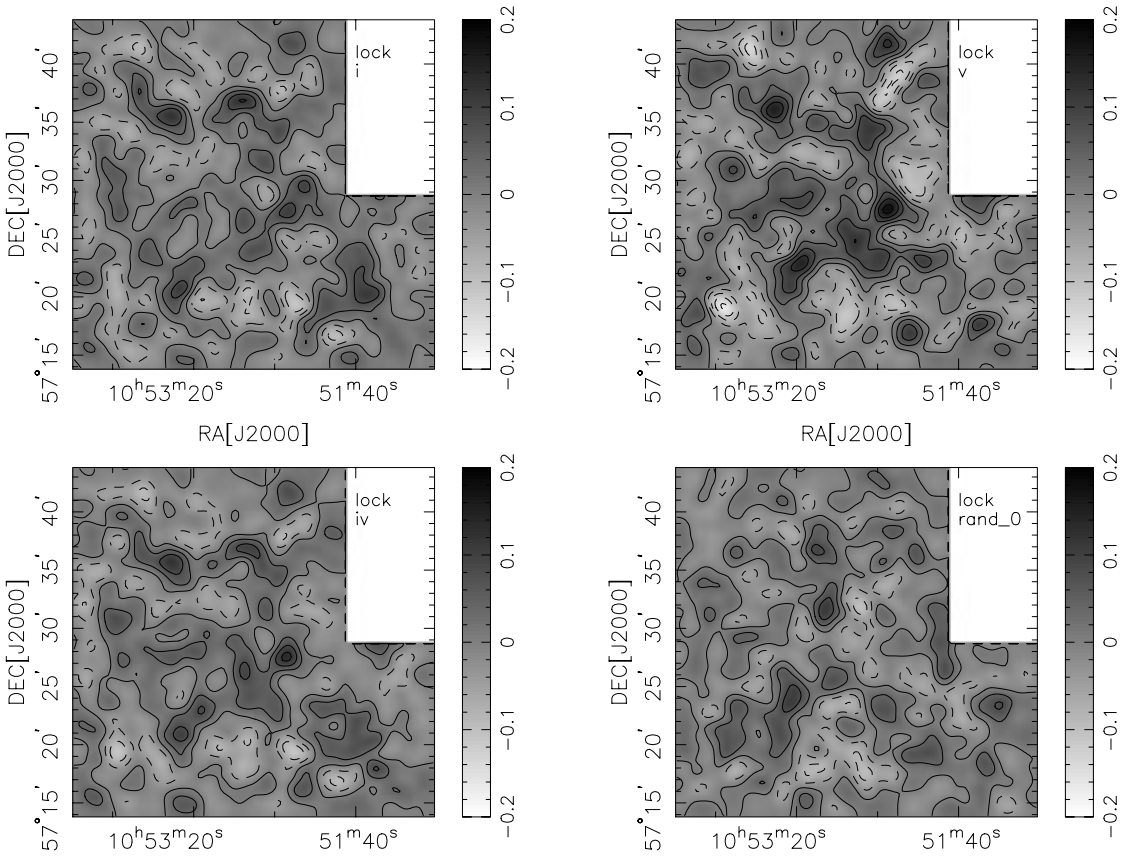

FIG. 1.—Upper panels show reconstructions of mass surface density $\kappa(=\Sigma/\Sigma_{\rm crit})$ made from the I- and V-band catalogs separately for Lockman field (pointing 1). Lower left panel shows the reconstruction from the composite IV catalog, and the lower right panel shows the reconstruction from the same catalog with randomized ellipticities, indicating the expected noise fluctuations caused by intrinsic random galaxy shapes. Reconstructions have been smoothed with a 45″ Gaussian filter. The wedge shows the calibration of the gray scale, and the contour separation is $0.04 \times \Sigma/\Sigma_{\rm crit}$.

show later, these trace the mass; thus, by focusing on the distribution of early-type galaxies, one can accurately forecast the distribution of mass in the universe.

As shown in § 2.2 of Paper II, with fluxes in two passbands one can reliably select bright early-type galaxies and assign them approximate redshifts. This is because early-type galaxies are the reddest galaxies at a given redshift. Thus, if we select galaxies of some color c, we will see a superposition of early-type galaxies at redshift z_E such that $c = c_E(z_E)$, and later types at their appropriate, but considerably higher, redshift. An $L \sim L_*$ early-type galaxy will appear much brighter than an $L \sim L_*$ late-type galaxy by about 3 mag, so with a judicious cut in red flux it is possible to isolate a bright early-type galaxy sample. At lens redshift higher than $z \simeq 0.4$, all galaxies with colors $V-I > 2.4$ are early-type galaxies, and it is unnecessary to apply any magnitude cut to exclude late types. We do, however, exclude galaxies with m_I fainter than 23.0. Figure 2 of Paper II shows $V-I$ color versus redshift for four galaxy types, and Figure 1 from the same paper shows counts predicted for all galaxy types and also the specific magnitude cut we employ at each redshift to ensure that only early-type galaxies remain in our sample. Table 2 shows the number of early-type lens galaxies per redshift slice ($dz = 0.1$) brighter than the magnitude cut (summed over all six pointings).

2.3. *Background (Source) Galaxy Sample*

The background sample was selected to lie in a range of significance $4 < \nu < 150$ (equivalent to limiting magnitudes of $m_I \simeq 25$ and $m_I \simeq 21$ for a point source). Shear estimates for each galaxy, $\hat{\gamma}_\alpha$ (for $\alpha = 1, 2$), were determined using the method described in Kaiser (2000) and Paper I. Weighted second moments were calculated from

$$q_\alpha = M_{\alpha lm} \int d^2\boldsymbol{r}\; S(\boldsymbol{r}) r_l r_m\, f(\boldsymbol{r})\,, \tag{1}$$

where f is flux; r is projected angular separation from the galaxy center; S is a Gaussian smoothing function to prevent the integral diverging at large radii; and the two constant matrices M_1 and M_2 are

$$M_{1lm} \equiv \begin{bmatrix} 1 & 0 \\ 0 & -1 \end{bmatrix}, \quad M_{2lm} \equiv \begin{bmatrix} 0 & 1 \\ 1 & 0 \end{bmatrix}. \tag{2}$$

Weighted second moment shapes and magnitudes of objects were measured using varying aperture photometry. The final number of galaxies per pointing and passband is shown in Table 3.

A "best" combined IV catalog was also created. This is a catalog containing galaxies that have been detected in *both* I and V images above a threshold significance (of 4ν). This is to ensure that any given "detection" is truly a real object. Shape information, i.e., shear estimates, are retained from the higher significance passband detection and discarded from the alternate passband. The galaxies tend to be detected at higher significance in the I-band images, and we find that the majority ($\simeq$80%) of galaxies in the combined IV catalog originate from the I catalog. The final number of

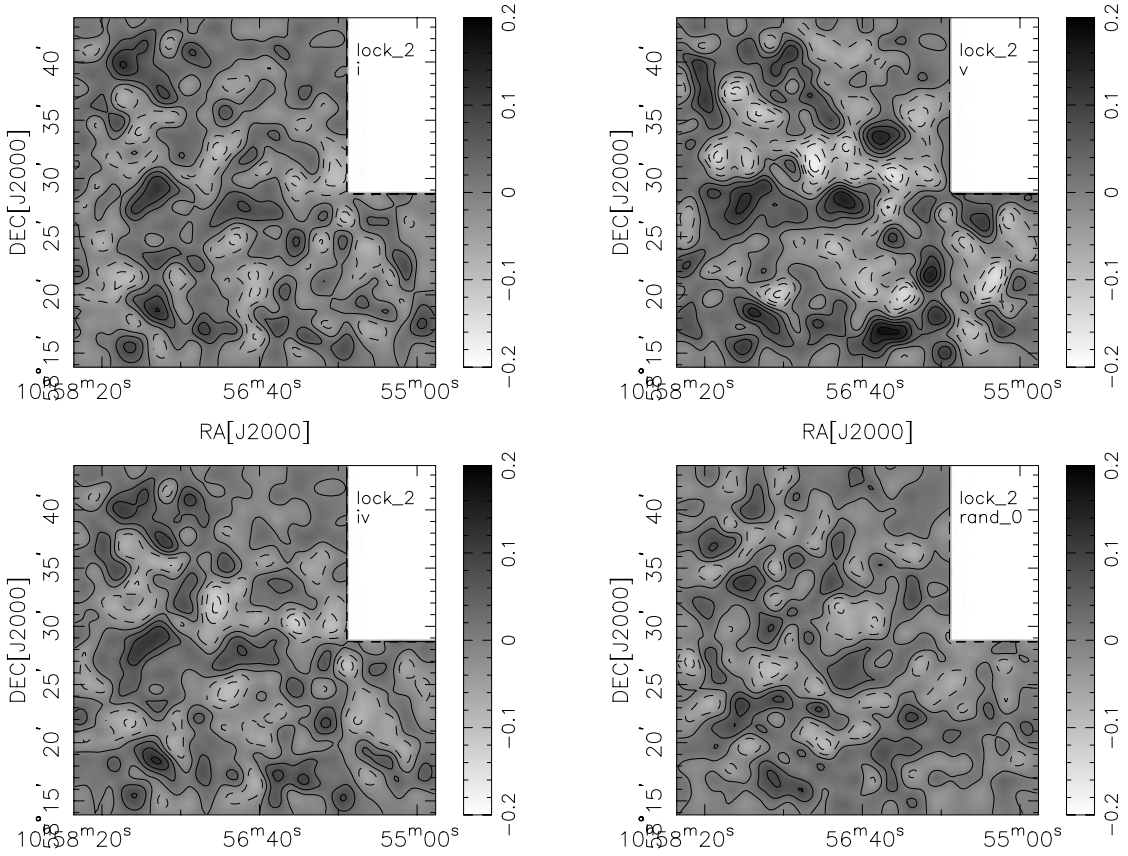

FIG. 2.—Same as Fig. 1, but for Lockman field (pointing 2)

objects in each IV catalog is shown in Table 3. (As discussed in Paper I, there are some low-level systematics still present in the catalogs. However, these are likely to have very little effect on the results presented in this paper for two reasons. First, in this paper we analyze the light-mass cross-correlation rather than the mass autocorrelation investigated in Paper I. Thus, any systematic component to the shear will not correlate with the light and is likely to average out. Second, we utilize mainly the IV catalog and this contains mostly galaxies originating from the I band, which was shown in Paper I to be less affected by systematics than the V band.)

From galaxy shear estimates, $\hat{\gamma}_\alpha$, we constructed two-dimensional mass surface density reconstructions in terms of the dimensionless quantity κ (where $\kappa = \Sigma/\Sigma_{\rm crit}$, the physical mass per unit area in units of the critical surface density). For any given lens and source galaxy redshift, the critical surface density, $\Sigma_{\rm crit}$, is the mass surface density required to refocus light. In the case of a distribution of background galaxy redshifts, $\Sigma_{\rm crit}$ becomes an average or effective mass surface density and is given by

$$\frac{1}{\Sigma_{\rm crit}} = \frac{4\pi G}{c^2}\,\frac{a_0\,\omega_l}{1+z_l}\,\langle\beta(z_l)\rangle\,, \tag{3}$$

where ω is comoving distance measured in units of the current curvature scale $a_0 = c/[H_0(1-\Omega_{m0}-\Omega_{\lambda 0})^{1/2}]$, and the dimensionless quantity $\langle\beta(z_l)\rangle$ is defined as

$$\langle\beta(z_l)\rangle \equiv \frac{\int_0^\infty dz_s\, n_s(z_s)\langle W_s(z_s)\rangle\beta(z_l, z_s)}{\int_0^\infty dz_s\, n_s(z_s)\langle W_s(z_s)\rangle}\,, \tag{4}$$

where $n_s(z)$ is the redshift distribution of the source galaxies, $\langle W_s(z_s)\rangle$ is the mean weight for source galaxies at redshift z_s, and where, finally,

$$\beta(z_l, z_s) \equiv \max\,[0, \sinh\,(\omega_s - \omega_l)/\sinh\,(\omega_s)]\,. \tag{5}$$

Physically, $\beta(z_l, z_s)$ is the ratio of the distortion induced by a lens at redshift z_l in an object at finite distance $\omega(z_s)$ relative to that for a fictitious source at infinite distance.

For the special case of a spatially flat cosmology, $\omega \to 0$ and $a_0 \to \infty$, but such that their product remains finite. In that case, $\sinh\,\omega \to \omega$, and $\langle\beta\rangle \equiv \langle\max\,(0, 1-\omega_l/\omega_s)\rangle$. For the limiting case of $\Omega_m = 1$, $\Omega_\lambda = 0$, $\omega(z) = 2[1 - 1/(1+z)^{1/2}]$ and, in the other extreme, for $\Omega_m \to 0$, $\Omega_\lambda \to 1$, $\omega(z) = z$.

Figures 1–6 show two-dimensional reconstructions of κ using galaxy shear estimates from the catalogs described in Table 3. The Kaiser & Squires (1993) reconstruction algorithm was used. This is a stable and fast reconstruction method that has very simply defined noise properties; essentially Gaussian white noise. As with all reconstruction methods, there is a tendency for noise to increase near the data boundaries. The upper panels show the reconstructions from catalogs made from the I- and V-band observations separately. The lower left panel shows the reconstruction from the composite IV catalog (our preferred catalog), and the lower right panel shows the reconstruction using a randomized catalog (containing the same galaxy positions as the original IV catalog but with randomly shuffled shear values), indicating the expected noise fluctuations caused by intrinsic random galaxy shapes. The mass reconstruction from the IV catalog is very similar to

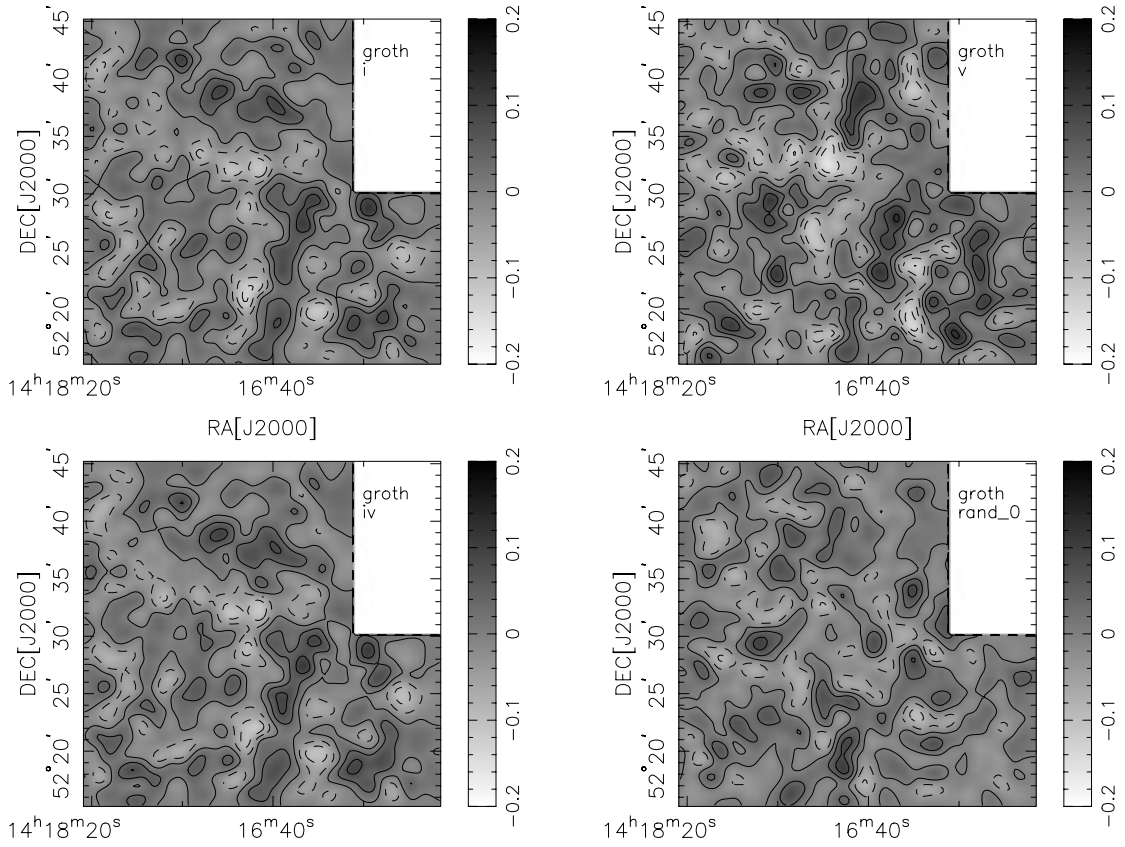

FIG. 3.—Same as Fig. 1, but for Groth field (pointing 1)

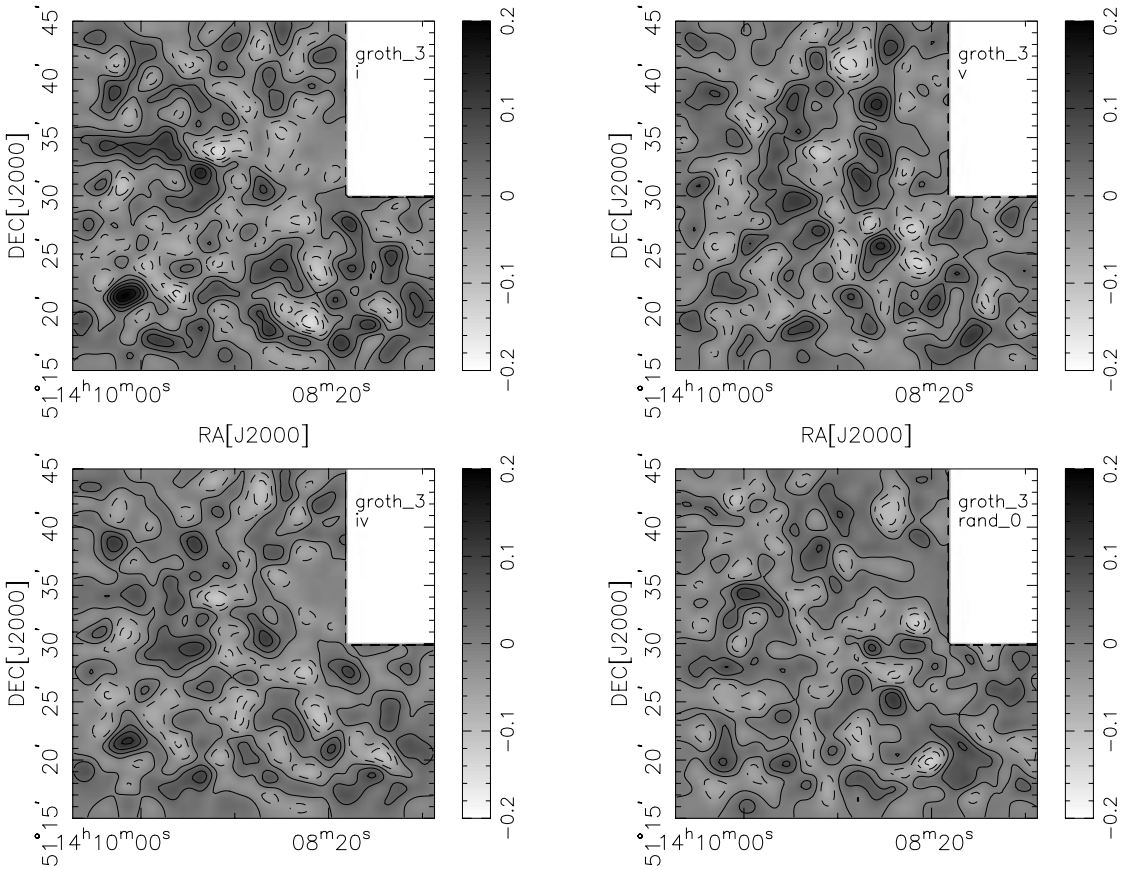

FIG. 4.—Same as Fig. 1, but for Groth field (pointing 3)

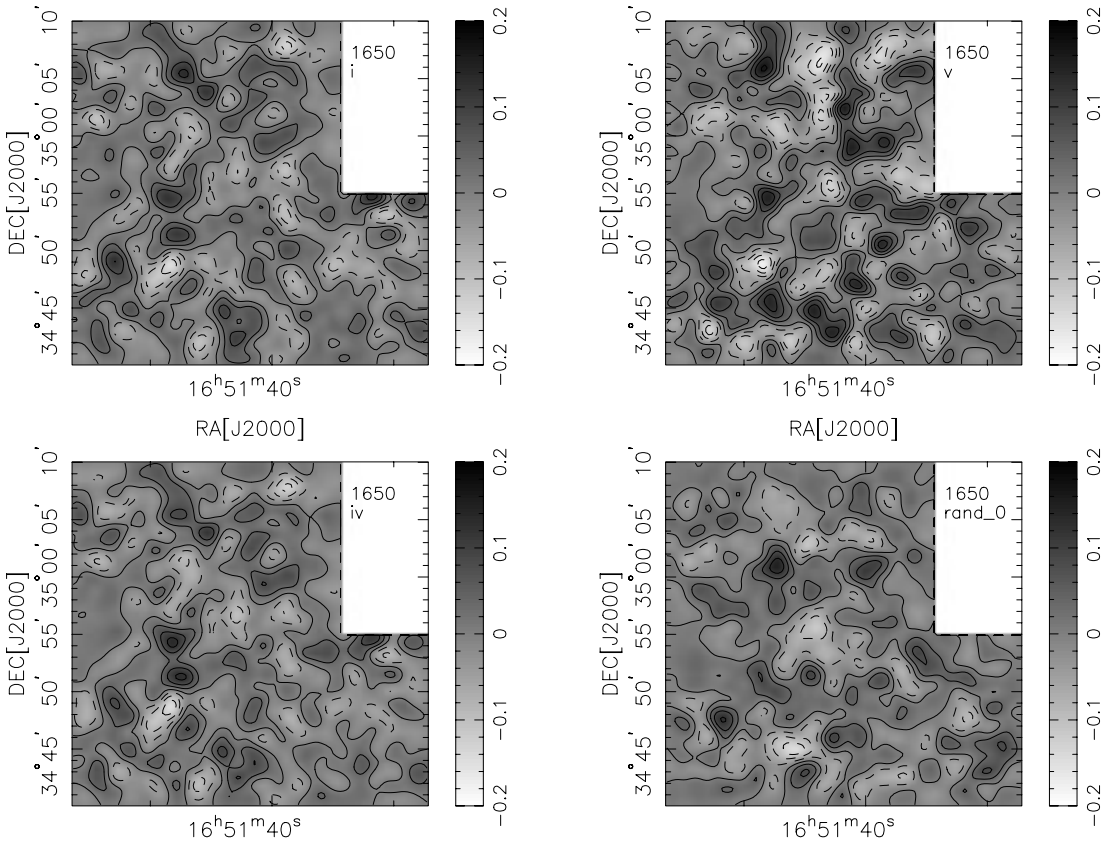

FIG. 5.—Same as Fig. 1, but for 1650 field (pointing 1)

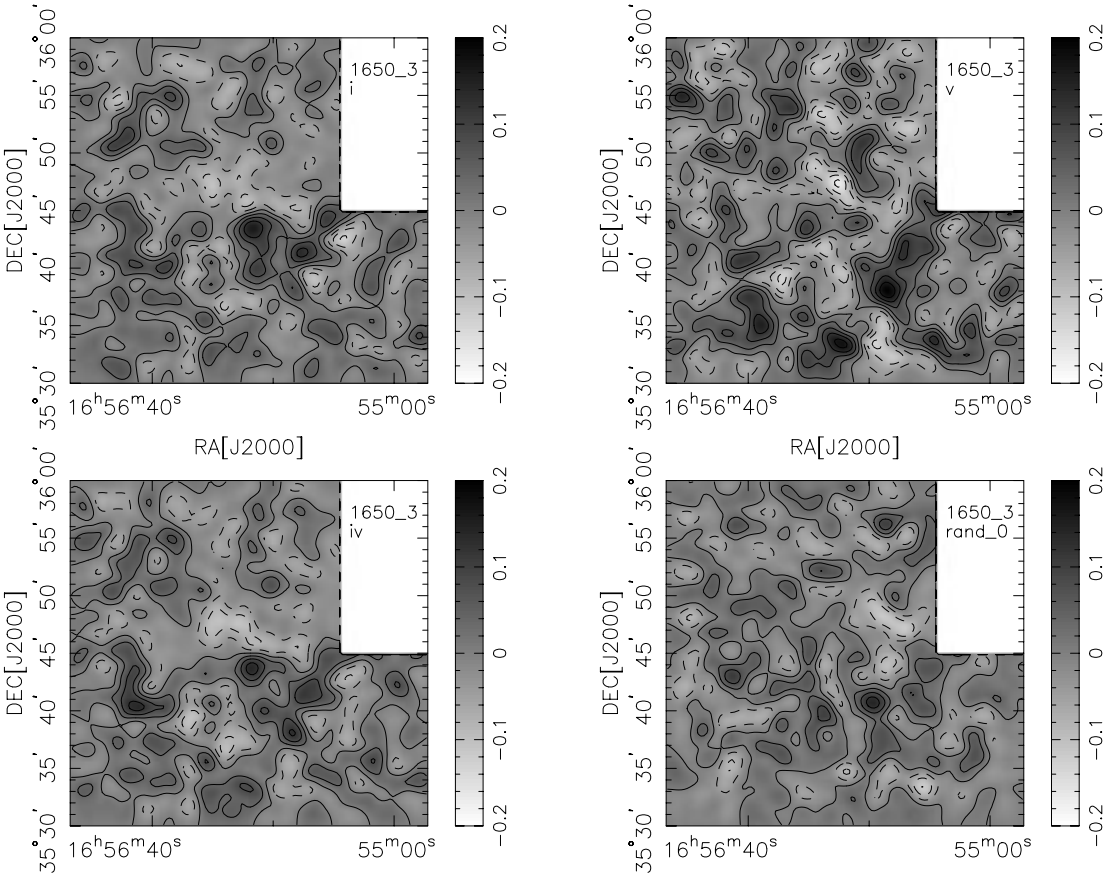

FIG. 6.—Same as Fig. 1, but for 1650 field (pointing 3)

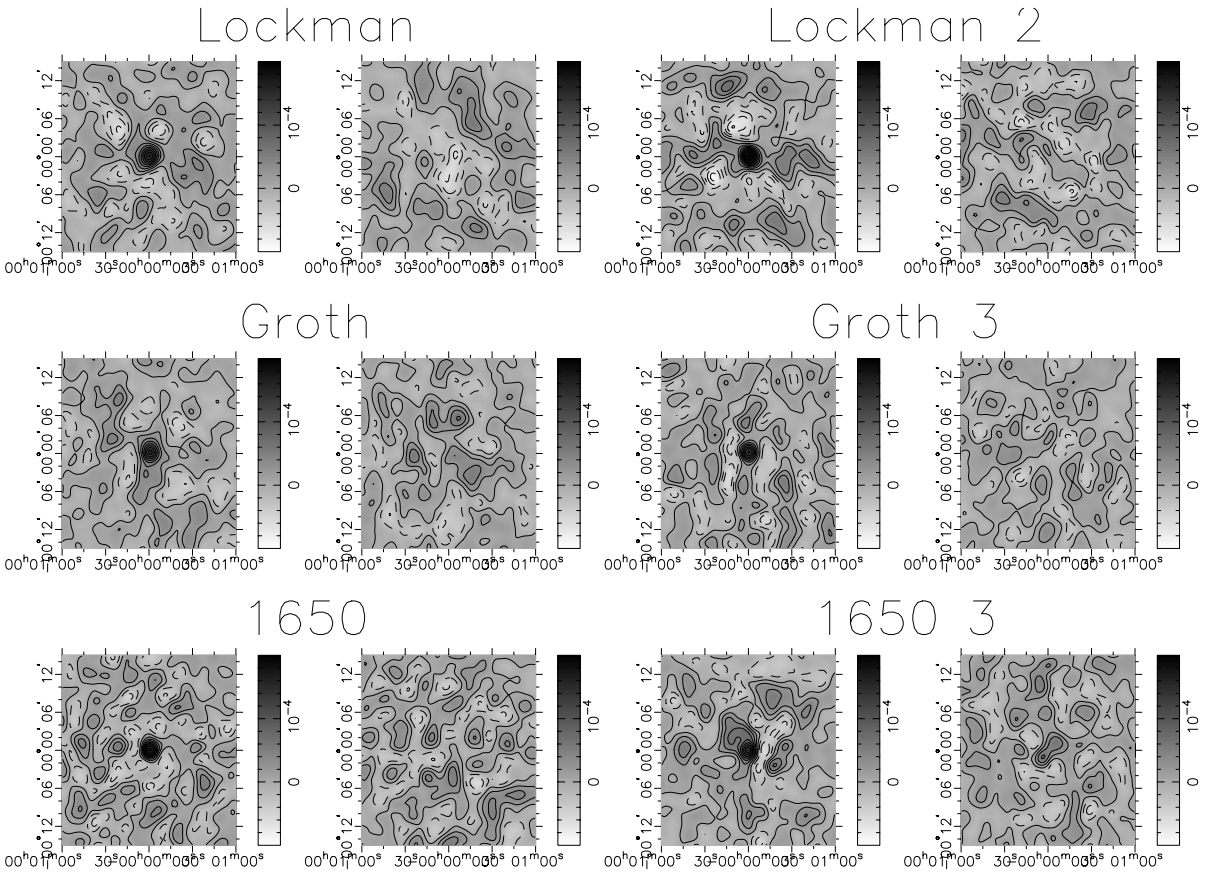

FIG. 7.—Cross-correlation of mass reconstruction from the V catalog with mass reconstruction from the I catalog (*left panel*) and with mass reconstruction from the randomized I catalog (*right panel*) for Lockman (*upper*) to 1650 (*lower*) fields.

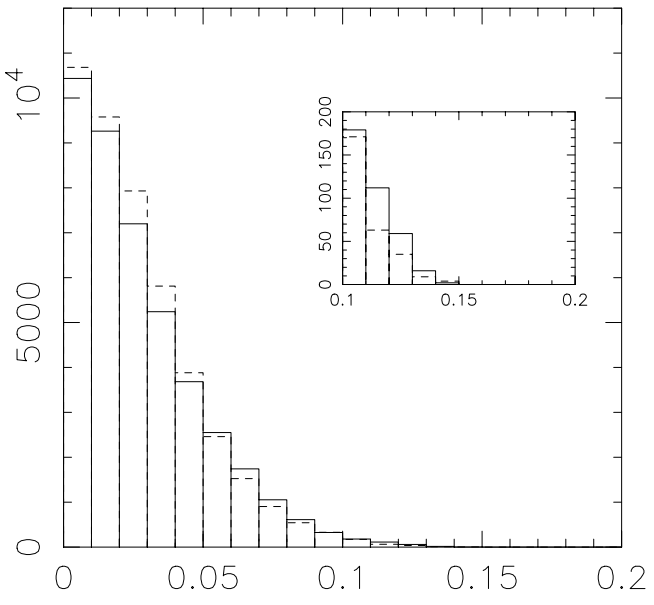

FIG. 8.—Histograms of absolute pixel values from the reconstructions of mass surface density κ using shear estimates from the IV catalogs (Figs. 1–6). The solid histogram describes originally positive pixels, and the dashed histogram describes originally negative pixels. The inset shows the contrast for extreme values. Clearly the distribution is very symmetrical. Notably, a highly positive tail is absent, indicating the absence of very overdense structures, e.g., rich clusters.

that from the I catalog as might be expected if the majority of objects originated from that catalog. The reconstructions have been smoothed with a 45″ Gaussian filter. The wedge shows the calibration of the gray scale, and the contour separation is $0.04 \times \Sigma/\Sigma_{\rm crit}$.

The first thing that one notices about the mass surface density reconstructions in Figures 1–6 is that mass structures are much more difficult to discern than for reconstructions of clusters. At first glance, it is often somewhat unclear as to whether any given peak (or trough) in the mass reconstruction is real or simply a spurious noise feature caused by discrete sampling of the background wallpaper of galaxies and their intrinsic ellipticities. It would be very difficult to quantify mass distributions directly from these maps.

The eye can be deceiving, however. The I and V reconstructions are actually extremely similar with regards to the positioning of the major mass distributions. Figure 7 shows the cross-correlation of the mass reconstruction from the V catalog with the mass reconstruction from the I catalog (*left panel*) and with the mass reconstruction from the I catalog with randomized shear values (*right panel*) for Lockman (*upper*) to 1650 (*lower*) pointings. In each case, there is a prominent peak at zero lag. The peak is significant at the ~ 6–$8\ \sigma$ level, depending on the pointing. That the I- and V-band signals are similar does not prove conclusively that galaxies in the I and V catalogs have been lensed by the same foreground mass structures (after all, the I and V

catalogs contain many of the same objects and might simply be subject to the *same* systematics), but it is certainly reassuring.

Figure 8 illustrates more quantitatively the difficulty of teasing true signal from the noise. This figure shows two histograms of absolute pixel value from the reconstructions of mass surface density κ using the shear estimates from all six *IV* catalogs (Figs. 1–6). The solid histogram describes originally positive pixels, and the dashed histogram describes originally negative pixels. The inset shows the contrast for extreme values. Clearly, the distribution is very symmetrical. Notably, a highly positive tail is absent, indicating the absence of very overdense structures, e.g., rich clusters.

In view of the difficulty of measuring mass *directly* from Figures 1–6, and since we have a large area containing many structures, it may be possible to better reveal the signal by cross-correlating light and mass. In the following section, we cross-correlate the luminosity associated with foreground galaxies with the mass inferred from the background galaxy shear estimates.

3. MASS AND LIGHT

3.1. *Mass Surface Density Predictions from Luminosity*

In this section we generate predictions of the dimensional mass surface density κ from *I*-band galaxy luminosity, assuming a constant M/L_B. The implicit assumption is that optical early-type galaxy luminosity is an unbiased tracer of the mass.

For a single galaxy with observed magnitude m_I, and for any cosmology, the contribution to an image of κ from a galaxy at redshift z_l, which falls in a pixel with solid angle $d\Omega$, is

$$\kappa\, d\Omega = \frac{M}{L_B}\,\frac{4\pi G M_\odot\, a_0}{c^2(10\mathrm{pc})^2}\,(1+z_l)^3 w_l \langle\beta(z_l)\rangle \times 10^{0.4[M_{B\odot}-m_I+K_{BI}(z_l)]}\,, \quad (6)$$

where M/L_B is in solar units, i.e., $h\, M_\odot/L_\odot$ [obtained from $\kappa = (M/dA)/\Sigma_{\rm crit}$, where A is area, $M/M_\odot = M/L \times L/L_\odot$, and $L/L_\odot = 10^{-0.4(M_B - M_{B\odot})}$, where $M_{B_\odot}$ is the absolute magnitude of the Sun in the B passband and where $K_{BI}(z) = K_I(z) - (M_B - M_I)_0$ is the combination of the conventional K-correction and the rest-frame color].

From equations (3) and (6), κ is a function of both lens and source galaxy redshift. The lens redshift is known fairly accurately from the $V-I$ color, but, in order to make an accurate prediction for the dimensionless surface density κ, it is necessary to have an accurate prediction for $\Sigma_{\rm crit}$ and hence to have an accurate model for the redshift distribution of the faint source galaxies.

The catalogs used here are not particularly deep, and there are nearly complete redshift samples that probe similar magnitude ranges. In Paper II the catalogs were compared to the SSA22 field sample from Cowie's (ongoing) galaxy survey (Cowie et al. 1994, 1996; Cowie, Songaila, & Barger 1999; G. Wilson, L. L. Cowie, A. J. Barger, & D. J. Burke 2001, in preparation). In both of our *I*- and *V*-band samples, the weight is distributed over a range of several magnitudes, with half of the weight attributed to galaxies brighter/fainter than $m_I \simeq 23.0$ and $m_V \simeq 24.2$. The very faintest galaxies lie beyond the completion limit of Cowie's sample, but the redshift distribution in a band 1 mag wide about the median magnitude is well determined. To a first approximation, the effect of variation of mean redshift with magnitude should cancel out, so one can adopt the central-band redshift distribution as appropriate for the full sample. At this magnitude, the samples are approximately 80% complete, and it is thought that the galaxies for which a redshift cannot be obtained lie predominantly around $z = 1.5$–2.0.

The redshift distribution was shown to be well modeled by

$$p(z) = 0.5z^2 \exp\,(-z/z_0)/z_0^3\,, \quad (7)$$

for which the mean redshift is $\bar{z} = 3z_0$ and the median redshift is $z_{\rm median} = 2.67z_0$. This is also the analytic form used by Wittman et al. (2000) and others and seems to adequately describe the data. To allow for incompleteness, we set the parameters n_0, z_0 of the model distribution to match the total number of galaxies in the Cowie sample (with and without secure redshifts) and to match the mean redshift with the unmeasurable objects assigned a redshift $z = 1.8$. Figure 4 of Paper II shows the redshift distribution for galaxies around $m_I = 23.0$ along with the incompleteness corrected model, which has redshift scale parameter $z_0 = 0.39$. The same calculation for galaxies selected in a 1 mag wide band around $m_V = 24.2$ yields a slightly smaller, though very similar, redshift parameter $z_0 = 0.37$. Thus, the *I* and *V* catalogs probe to similar depth in redshift.

In Figure 9, we plot $1/\Sigma_{\rm crit}$ as a function of lens redshift for three cosmologies using equation (7) as the source galaxy distribution. The dot-dashed line is flat lambda ($\Omega_{m0} = 0.3$, $\Omega_{\lambda 0} = 0.7$), the solid line is Einstein–de Sitter ($\Omega_{m0} = 1.0$, $\Omega_{\lambda 0} = 0.0$), and the dashed line is open baryon ($\Omega_{m0} = 0.05$, $\Omega_{\lambda 0} = 0.0$). The values of $1/\Sigma_{\rm crit}$ for the flat lambda case are shown in Table 2 as a function of z for redshift intervals $dz = 0.1$. We return to the dependence of M/L ratio on cosmology in § 4.1.

To obtain the total mass surface density along the line of sight out to $z = 1$, we use Table 2 to calculate $\kappa = \Sigma/\Sigma_{\rm crit}$ for each redshift slice individually and then sum the slices together. One could directly compare κ predicted from the light to κ from galaxy shear estimates obtained in § 2.3.

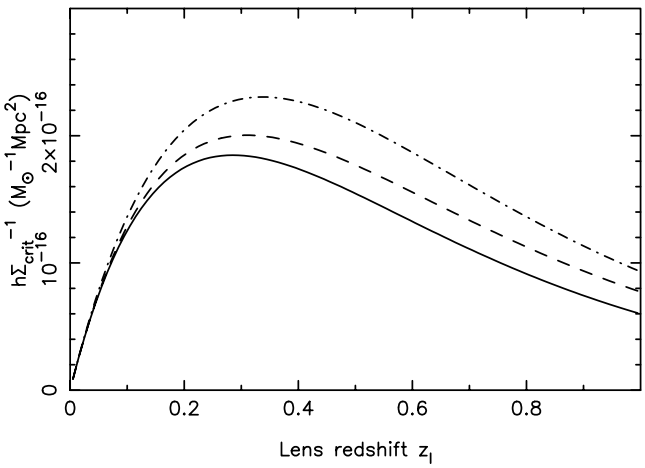

FIG. 9.—Inverse critical surface density, $1/\Sigma_{\rm crit}$, as a function of redshift and cosmology using the analytic approximation to an $m_I = 23$ source galaxy redshift distribution. The solid line is Einstein–de Sitter ($\Omega_{m0} = 1.0$, $\Omega_{\lambda 0} = 0.0$); the dashed line is open baryon ($\Omega_{m0} = 0.05$, $\Omega_{\lambda 0} = 0.0$); and the dot-dashed line is flat lambda ($\Omega_{m0} = 0.3$, $\Omega_{\lambda 0} = 0.7$).

However, to ensure that our κ-from-light prediction is subject to the same finite-field bias and other unknown systematics as the κ-from-shear reconstructions, we first make a shear field image prediction from the constant M/L_B prediction and then sample this at the actual positions of our faint galaxies to generate a synthetic catalog (that which would have been observed with no intrinsic random shape or measurement noise), and then generate a reconstruction from that synthetic catalog. To match the spatial resolution to that of the real reconstructions (a 45″ Gaussian) we generate the predicted shear with smoothing scale $45''/\sqrt{2}$ and create the reconstruction from the synthetic catalog with the same smoothing. While correctly accounting for the finite field effect on structures within the field, the actual shear may still feel some effect from structures outside of the field.

The upper left panels of Figures 10–15 show dimensionless surface mass density κ-from-light generated in this manner. We assumed $M/L_B = 300\ h\ M_\odot/L_\odot$. The mean has been subtracted from each image. The wedge shows the calibration of the gray scale, and the contour separation is $0.007 \times \Sigma/\Sigma_{\rm crit}$.

3.2. *Mass-Light Cross-Correlation*

In this section, we cross-correlate light with mass. Our first aim is to test the hypothesis of a constant mass-to-light ratio that is independent of scale and also, later, to determine the value of M/L_B, the constant of proportionality between mass and light. That is to say, we are comparing the lower left panels of Figures 1–6 with the upper left panels of Figures 10–15. We also require an estimate of uncertainties inherent in the reconstruction of κ from the galaxy shear estimates. To obtain this we create an ensemble of 32 reconstructions for each pointing using shear values measured from the *IV* catalog but shuffled randomly.

The left panel of Figure 16 shows the cross-correlation of light with mass averaged over all six pointings. In computing this, we padded the source images with zeros to twice the original size. The right panel of Figure 16 shows the cross-correlation of light with an average over randomized catalog reconstructions. There is a strong cross-correlation peak at zero lag for the real data, which is not present for the randomized data.

The mass-to-light ratio, M/L_B, at zero lag is calculated by minimization of

$$\chi^2 = \sum_i \frac{(y_i - M/L_B\, x_i)^2}{\sigma_i^2}\,, \tag{8}$$

where the sum is over the six pointings, the light autocorrelation $x_i = \Sigma_{\rm pix}\, \kappa_l\, \kappa_l/N_{\rm pix}$, the mass-light cross-correlation $y_i = \Sigma_{\rm pix}\, \kappa_m\, \kappa_l/N_{\rm pix}$, and the uncertainty is calculated from the ensemble of 32 randomized catalogs ($\sigma_i^2 = \sum (y_i^{\rm rand})^2/N_{\rm rand}$). Minimizing χ^2 with respect to M/L_B,

$$\frac{M}{L_B} = \frac{\sum_i x_i\, y_i/\sigma_i^2}{\sum_i x_i^2/\sigma_i^2}\,. \tag{9}$$

The uncertainty in M/L_B is

$$\sigma_{M/L_B} = \frac{1}{\sqrt{(\sum_i x_i^2/\sigma_i^2)}}\,. \tag{10}$$

The significance, estimated as the strength of the zero-lag correlation relative to the rms found from the ensemble of randomized catalogs is 5.2 σ (Table 4). That early-type galaxy luminosity and total mass show such a strong correlation is the central result of this paper. The correlation strength at zero lag implies a $M/L_B = 237 \pm 45\ h\ M_\odot/L_\odot$. The error is a 1 σ statistical uncertainty only and does not include any systematic error introduced into $1/\Sigma_{\rm crit}$ because of lack of knowledge about the redshift distribution of the source galaxies.

3.3. *Mass-Light Cross-Correlation Profiles*

To determine how M/L ratio varies with scale, we examine the profile of the luminosity-mass cross-correlation and luminosity autocorrelation. Figure 17 shows the azimuthally averaged profile of the mass-luminosity cross-correlation function (*open circles with error bars*) and the luminosity autocorrelation function (*filled circles*). The luminosity autocorrelation has been normalized to 1, and in normalizing the mass-luminosity cross-correlation function, we have adopted $M/L_B = 250\ h\ M_\odot/L_\odot$, similar to that obtained at zero lag in § 3.2. The error bars were calculated from our ensembles of 32 noise reconstructions. It is apparent from Figure 17 that although mass and luminosity do appear to trace each other, the profile is noisy, and thus it is difficult to judge if the profiles have similar shape.

In the upper left panel of Figure 18 we show the combined azimuthally averaged profile of the mass-luminosity cross-correlation function averaged over all six pointings (*open circles*) and the corresponding luminosity autocorrelation function (*filled circles*). Again, the luminosity autocorrelation has been normalized to 1, and in normalizing the mass-luminosity cross-correlation function we have adopted $M/L_B = 250\ h\ M_\odot/L_\odot$.

We see from Figure 18 that the cross-correlation and autocorrelation functions have very similar profiles. Thus, it appears that early-type galaxies trace the mass rather faithfully. We note that the profile in Figure 18 was obtained from smoothed images. The smallest scale over which mass/luminosity is being averaged is therefore $\simeq 45''$. We conclude therefore that on scales $\geq 45''$ our results are consistent with early-type galaxies tracing mass.

3.4. *Mass and Light as a Function of Redshift*

In this section we investigate M/L, the constant of proportionality between mass and light, as a function of redshift. We divide our data into three slices, each of size width $dz = 0.3$ (Table 4) and analyze each slice separately.

Figures 10–15 show the dimensionless surface mass density prediction κ-from-light generated as described in § 3.1. The remaining three panels in each figure show κ-from-light summed over three redshift slice intervals centered on $z = 0.2$, $z = 0.5$, and $z = 0.8$ rather than the sum over all nine redshift intervals described in § 3.1. We again assume $M/L_B = 300\ h\ M_\odot/L_\odot$ and use equations (3) and (6). Luminosity is binned into equal angular-size pixels, and we note that since our field of view corresponds to a different physical extent with redshift ($2.32\ h^{-1}$ Mpc at $z = 0.1$; $9.82\ h^{-1}$ Mpc at $z = 0.9$), the bin size is similarly a function of redshift. It is apparent from Figures 10 to 15 that most of the κ-from-light signal originates at low and intermediate redshift.

This effect can also been seen in Figure 19. The left panels show the cross-correlation of light with mass averaged over all six pointings as a function of redshift. The right panels show the cross-correlation of light with an average over

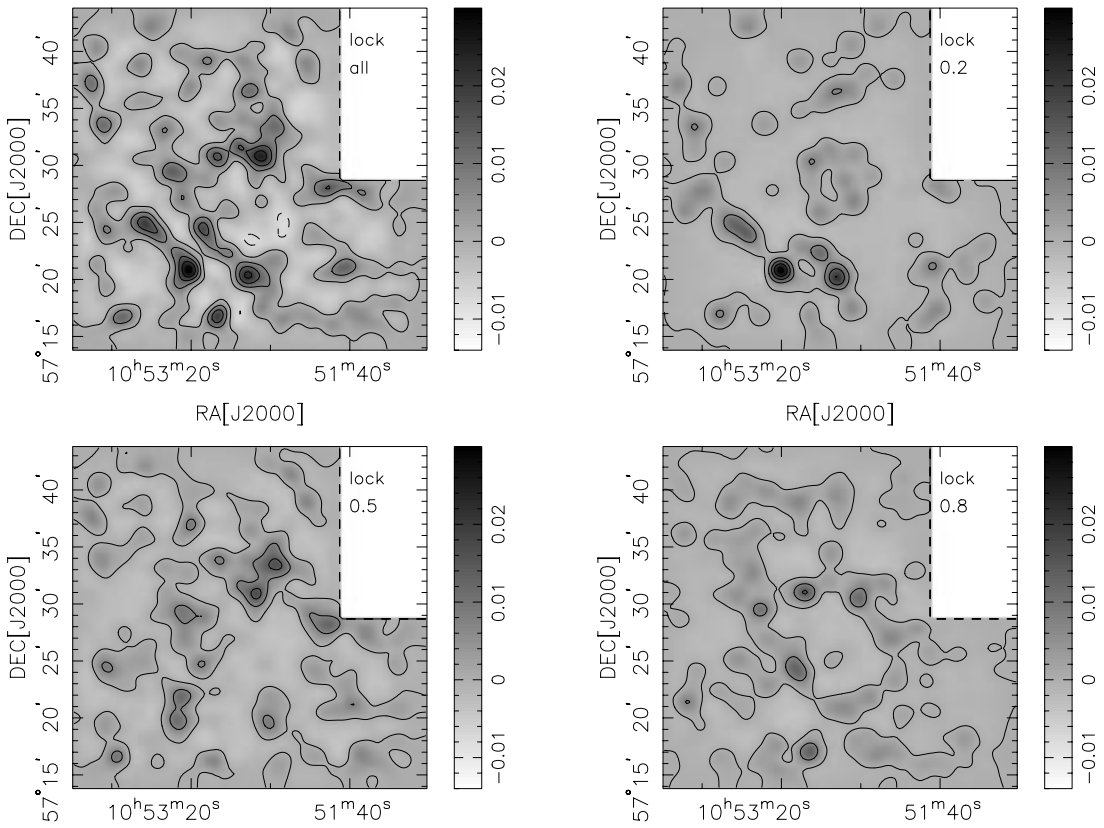

FIG. 10.—Upper left panel shows the predicted mass surface density using early-type galaxies selected by $V-I$ color, and $M/L_B = 300\,h\,M_\odot/L_\odot$ (see § 3.1 for details) for Lockman field (pointing 1). The image has been smoothed with a 45″ Gaussian filter. The mean has been subtracted from the image. The wedge shows the calibration of the gray scale, and the contour separation is $0.007 \times \Sigma/\Sigma_{\rm crit}$. The remaining three panels show the predicted surface mass density using early-type galaxies and $M/L_B = 300\,h\,M_\odot/L_\odot$ but subdividing the galaxies into $z = 0.2, 0.5, 0.8 \pm 0.15$.

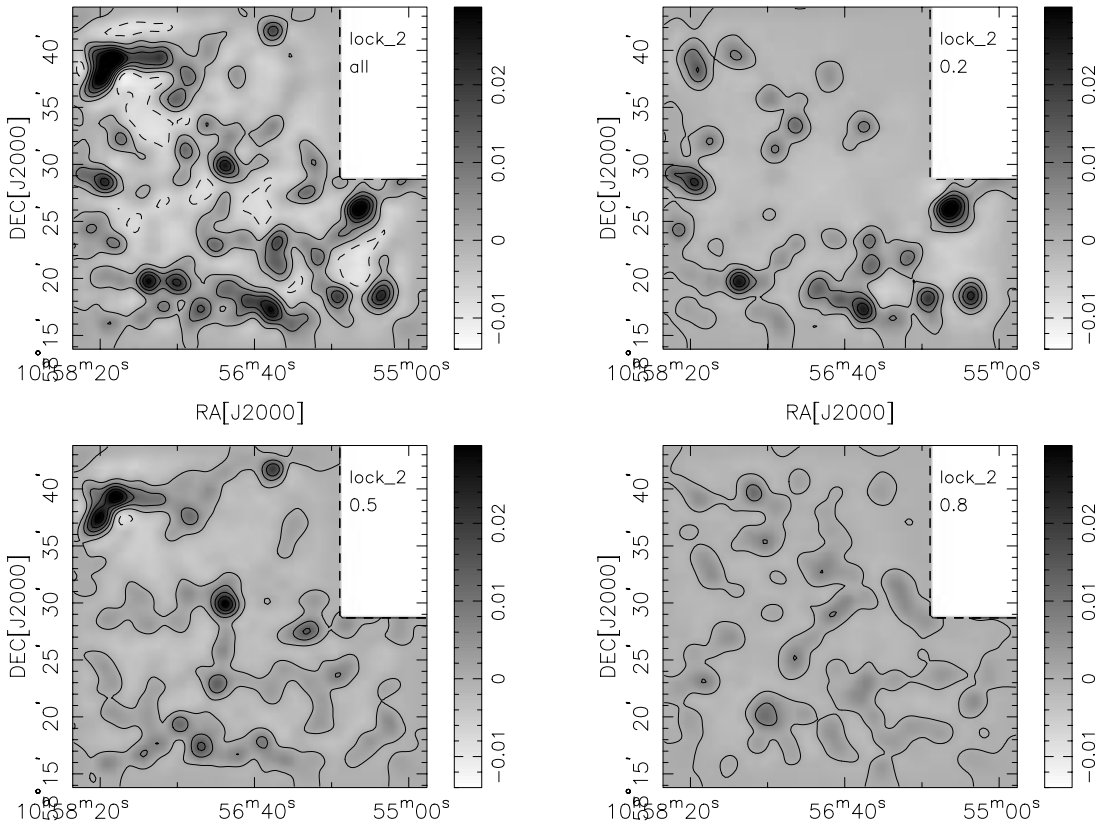

FIG. 11.—Same as Fig. 10, but for Lockman field (pointing 2)

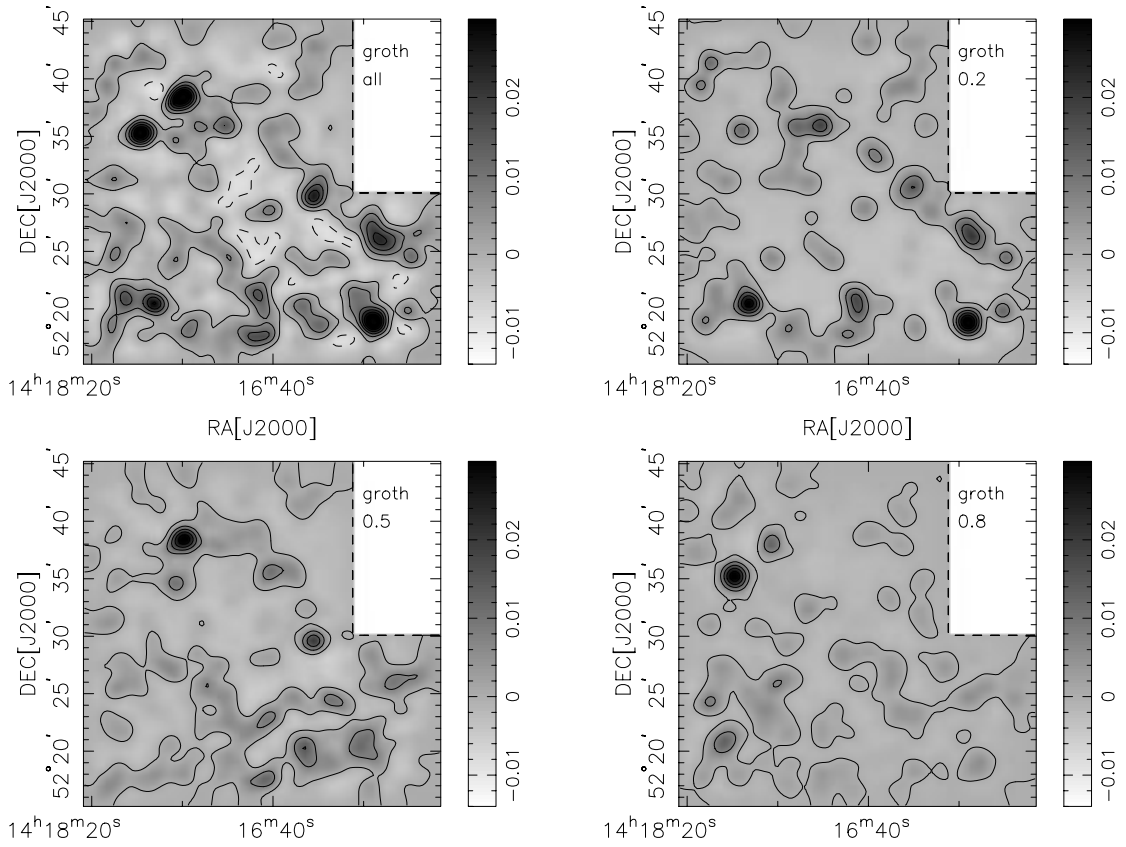

FIG. 12.—Same as Fig. 10, but for Groth field (pointing 1)

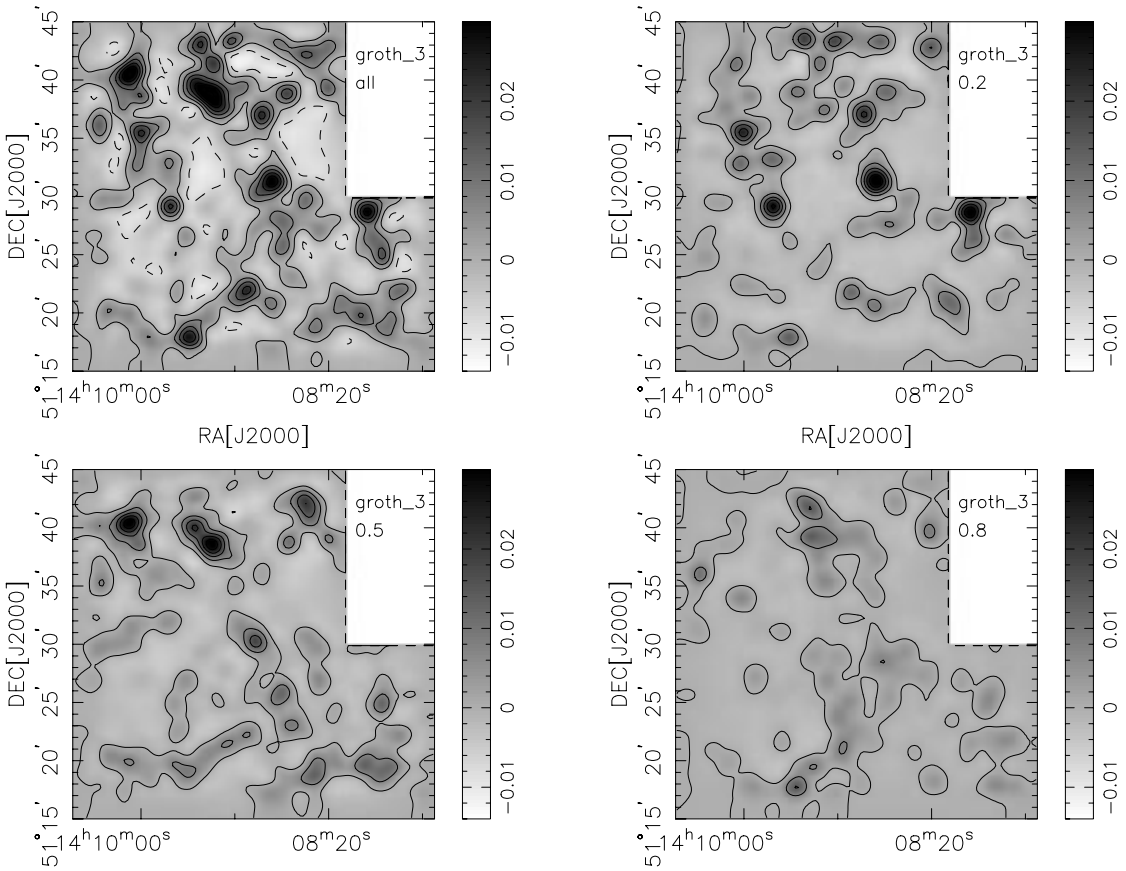

FIG. 13.—Same as Fig. 10, but for Groth field (pointing 3)

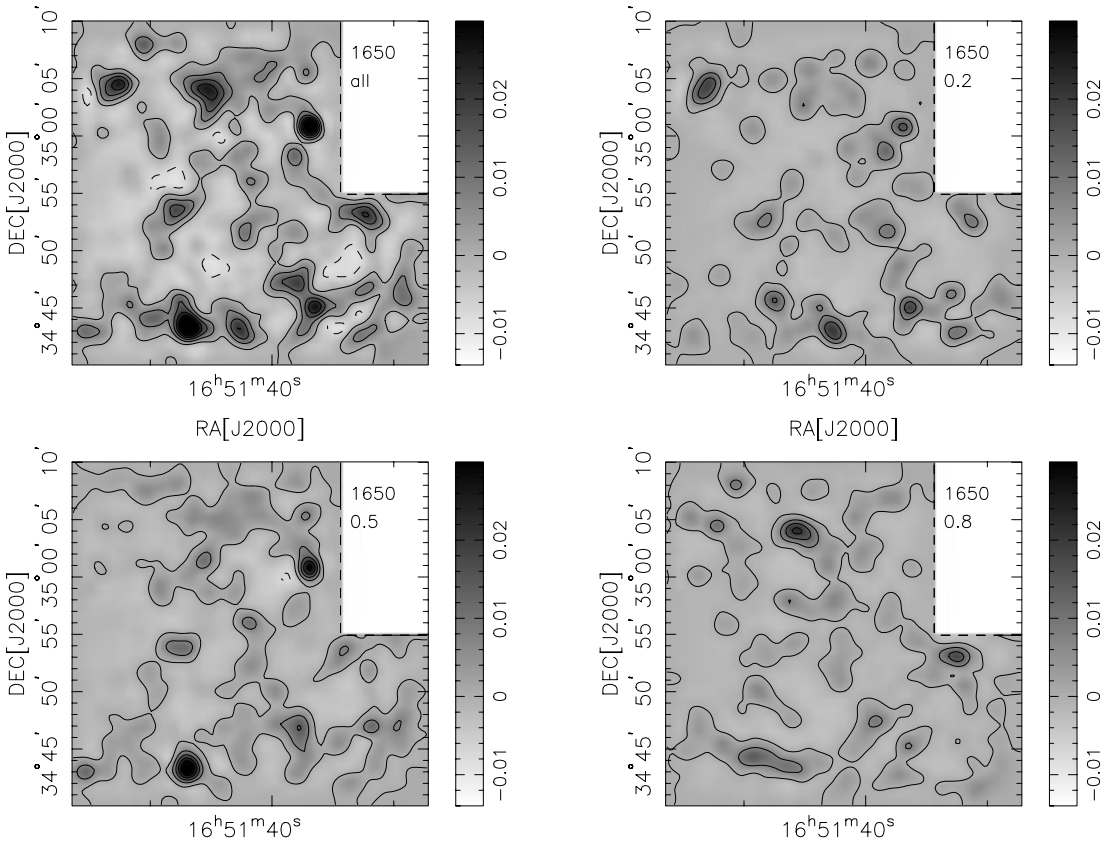

FIG. 14.—Same as Fig. 10, but for 1650 field (pointing 1)

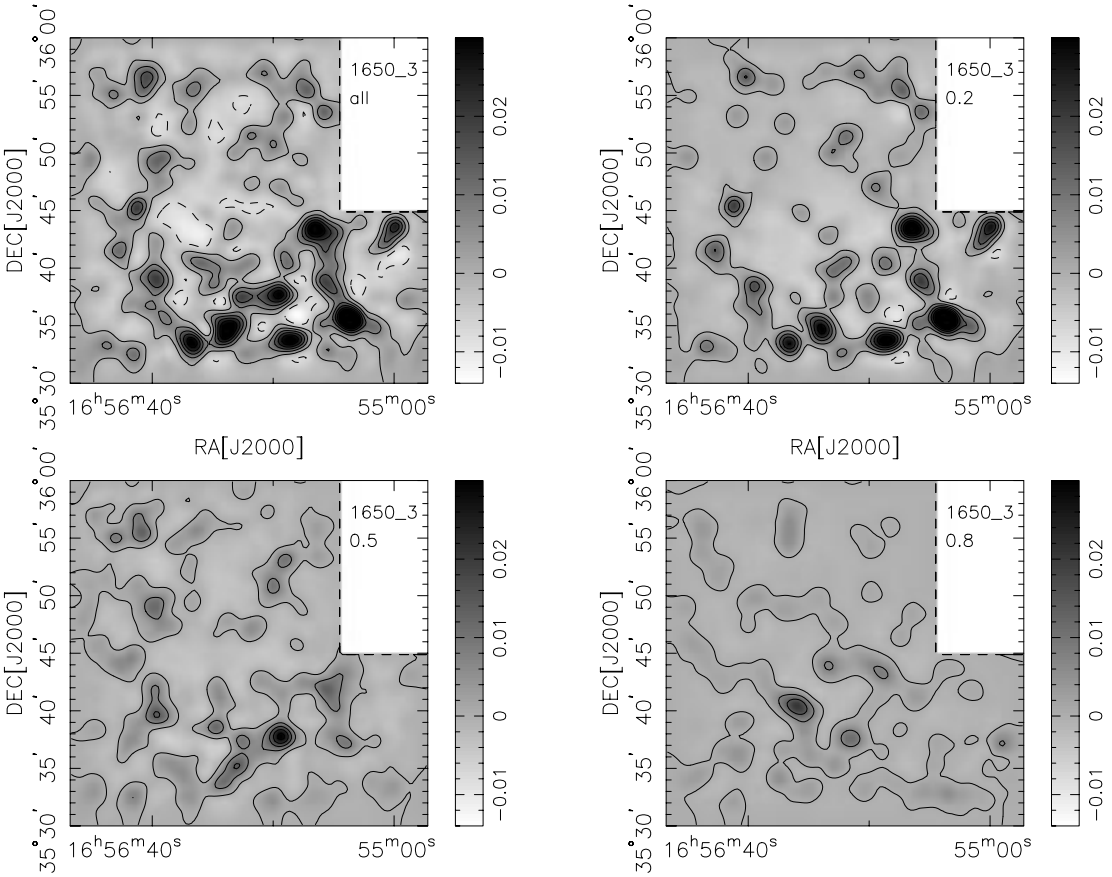

FIG. 15.—Same as Fig. 10, but for 1650 field (pointing 3)

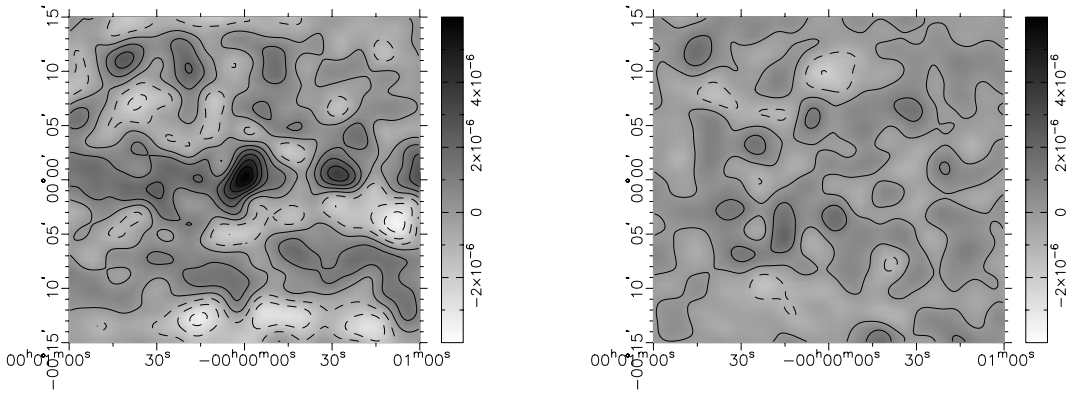

FIG. 16.—Cross-correlation of light with mass reconstruction (*left panel*) and with randomized catalog reconstruction (*right panel*). Contour separation is 1×10^{-6}, and the peak at zero lag is significant at the 5.2 σ level.

randomized shear catalog reconstructions. The slices centered on redshifts $z = 0.2$ and $z = 0.5$ show a strong cross-correlation peak at zero lag. The correlation strength at zero lag implies $M/L_B = 353 \pm 67\ h\ M_\odot/L_\odot$ for $z = 0.2$ with 5.3 σ significance and $M/L_B = 272 \pm 75\ h\ M_\odot/L_\odot$ for $z = 0.5$ with 3.6 σ significance (Table 4). The highest redshift slice shows no such peak and M/L_B consistent with zero ($-60 \pm 143\ h\ M_\odot/L_\odot$).

Figure 18 shows the azimuthally averaged profile of the mass-luminosity cross-correlation function (*open circles with error bars*) and the luminosity autocorrelation function (*filled circles*). The redshift interval is marked on each panel. Again, the luminosity autocorrelation has been normalized to 1, but for better comparison of the profiles, in normalizing the mass-luminosity cross-correlation function here, we have adopted a higher $M/L_B = 300\ h\ M_\odot/L_\odot$, more similar to that obtained at zero lag (rather than the $M/L_B = 250\ h\ M_\odot/L_\odot$ used for the whole sample in § 3.3). As before, uncertainties were calculated from 32 reconstructions using randomly shuffled shear values from our *IV* catalog.

There is perhaps some very slight evidence from Figure 18 that the mass-luminosity profile might be more extended than the luminosity-luminosity profile. An extended mass-luminosity profile would be expected if (1) any mass associated with late-type galaxies were nonnegligible and if (2) one takes into account the known fact that late-type galaxies are clustered around early-type galaxies (Davis & Geller 1976) but are more weakly clustered than early types around early types. A more realistic scenario, therefore, might include both early- and late-type galaxies, with a slightly lower M/L_B for early-type galaxies than quoted here, and an additional much lower but nonzero M/L_B for late types (the mass associated with late types cannot be dominant compared to the early types or we would not see such a strong mass–to–early-type–luminosity correlation in Fig. 16). Further data will be required to determine conclusively whether the mass-luminosity profile is actually extended and not simply a noise artifact. For now, however, we conclude, that within the uncertainties of this data set, we find no evidence for (early-type galaxy) luminosity and (total) mass segregation: it does appear that early-type galaxies trace the mass very similarly at all redshifts.

We note from Figure 18 that the uncertainties increase with increasing redshift. This is easily understandable when one realizes from equation (9) that, if the pointings have similar noise properties as they do here, the mass-light correlation essentially consists of the product of κ-from-shear and κ-from-light divided by the product κ-from-light squared:

$$\frac{M}{L_B}\,\frac{\Sigma_{\rm pix}\,\kappa_m\,\kappa_l}{\Sigma_{\rm pix}\,\kappa_l\,\kappa_l}\,. \tag{11}$$

TABLE 4

M/L_B VALUES AT ZERO LAG

Ω_{m0}	$\Omega_{\lambda 0}$	Lens Redshift	Number Lens	$\Sigma_{\rm crit}^{-1}$ ($\times 10^{-16}\ h^{-1}$ Mpc$^2\ M_\odot^{-1}$)	M/L_B	ν
			Flat Lambda			
0.3.....	0.7	0.5 ± 0.45	5440	1.91	237 ± 45	5.2
0.3.....	0.7	0.2 ± 0.15	680	2.08	353 ± 67	5.3
0.3.....	0.7	0.5 ± 0.15	3234	2.10	272 ± 75	3.6
0.3.....	0.7	0.8 ± 0.15	1526	1.44	−61 ± 143	−0.4
			Einstein–de Sitter			
1.0.....	0.0	0.5 ± 0.45	5018	1.39	294 ± 60	4.9
1.0.....	0.0	0.2 ± 0.15	526	1.72	385 ± 82	4.7
1.0.....	0.0	0.5 ± 0.15	2966	1.54	376 ± 101	3.7
1.0.....	0.0	0.8 ± 0.15	1526	0.98	−93 ± 211	−0.4

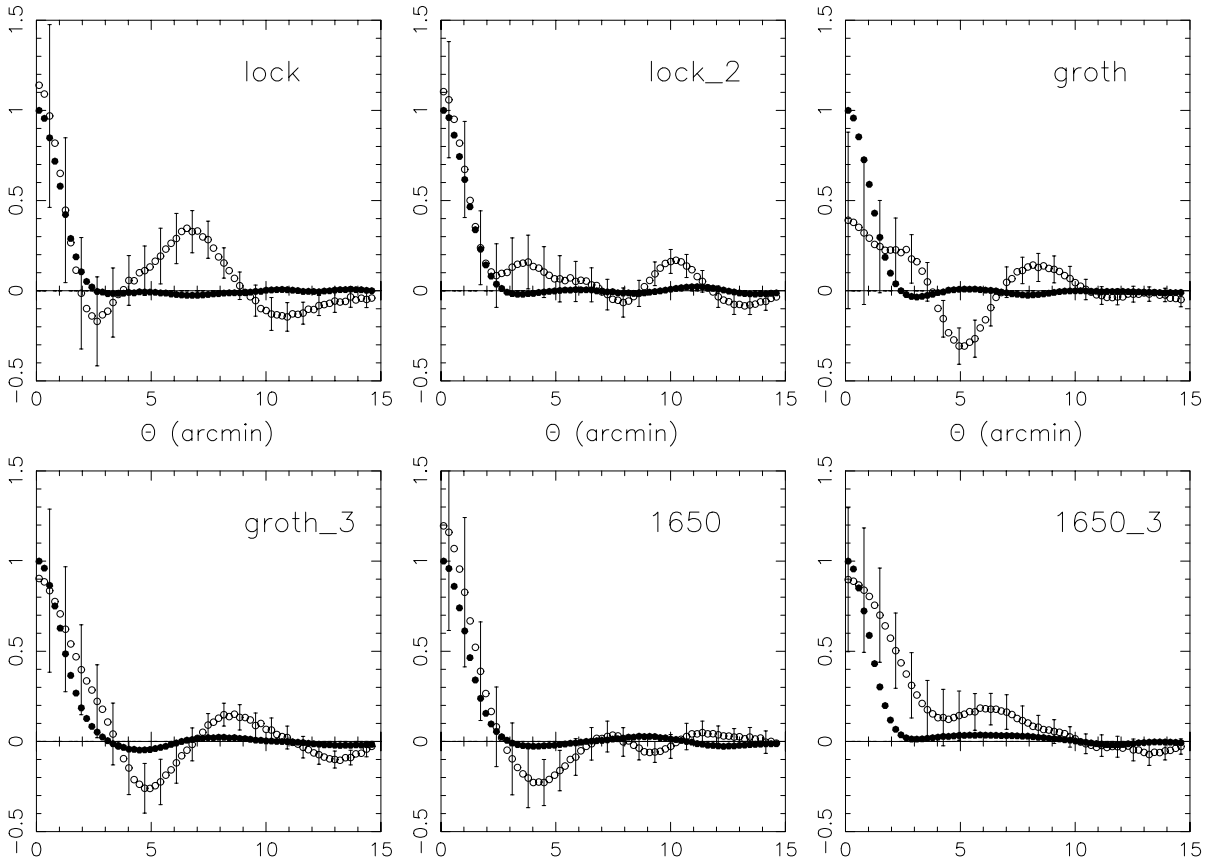

FIG. 17.—Azimuthally averaged profile of the mass-luminosity cross-correlation function (*open circles with error bars*) and the luminosity autocorrelation function (*filled circles*). In normalizing the mass-luminosity cross-correlation function, we have adopted $M/L_B = 250\ h\ M_\odot/L_\odot$. For clarity, only every third error bar is plotted.

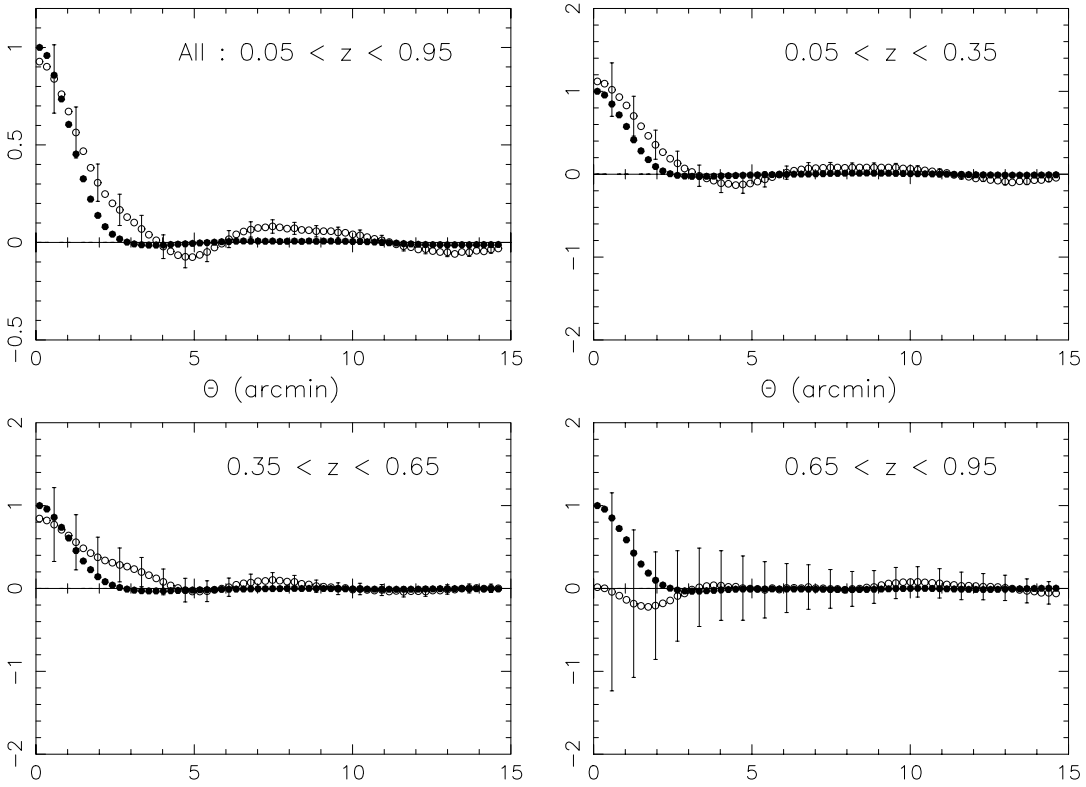

FIG. 18.—Azimuthally averaged profile of the mass-luminosity cross-correlation function from Fig. 16 (*open circles with error bars*) and the luminosity autocorrelation function (*filled circles*). Upper left panel is for all galaxies (adopting a normalization $M/L_B = 250\ h\ M_\odot/L_\odot$); other panels are for redshift intervals as marked (adopting a normalization $M/L_B = 300\ h\ M_\odot/L_\odot$). Note change of abscissa scale. For clarity, only every third error bar is plotted.

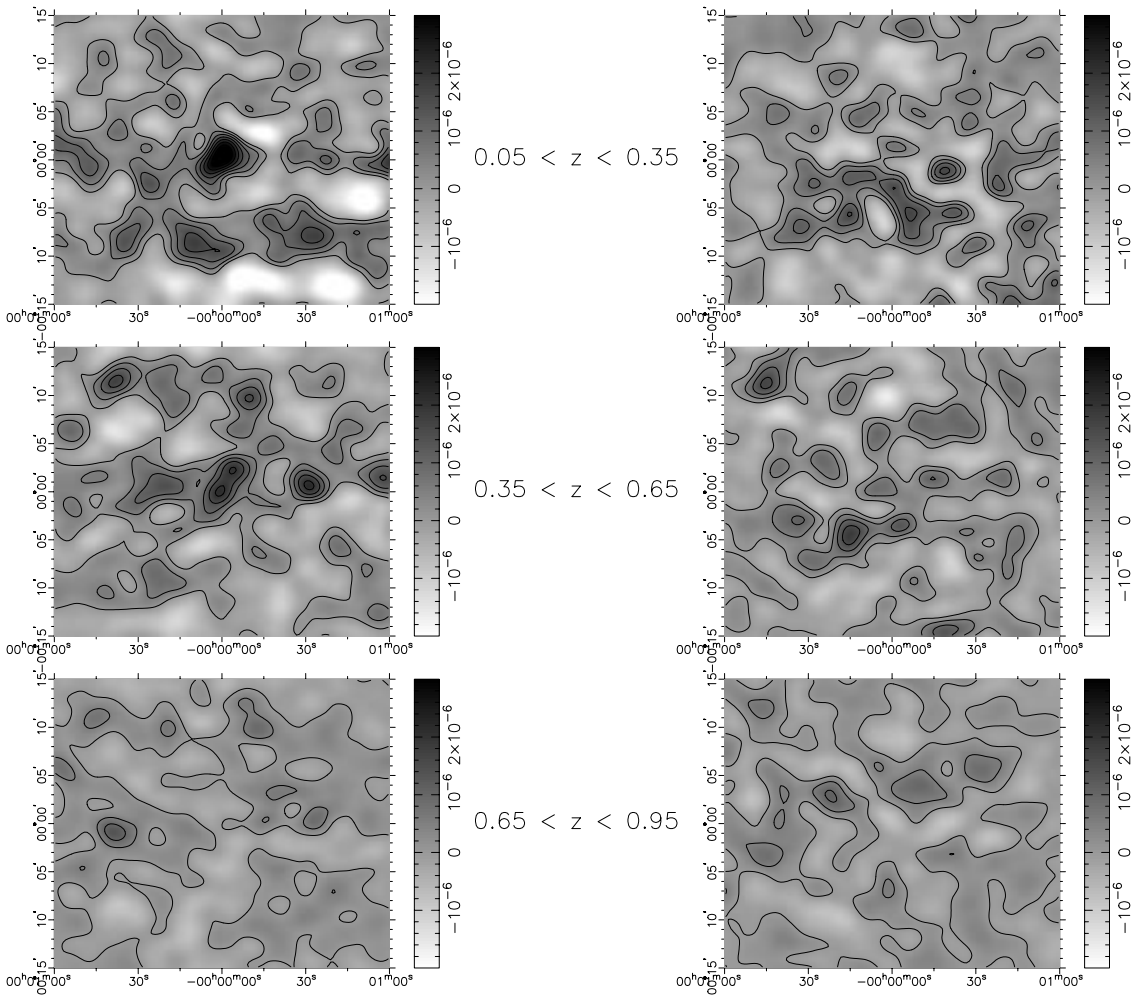

FIG. 19.—Same as Fig. 16, but cross-correlation of light from galaxies in redshift intervals $z = 0.2, 0.5, 0.8 \pm 0.15$ with mass reconstruction (*left panel*) and with randomized catalog reconstruction (*right panel*). The contour separation is 5×10^{-7}. A correlation is seen between light and mass for galaxies at low and intermediate redshifts, but no correlation is apparent for galaxies in the highest redshift interval.

Each factor of κ-from-light (eq. [6]) contains a factor of $1/\Sigma_{\rm crit}$, which at high redshifts becomes very small (Fig. 9). Thus, for higher redshift lenses, one is dividing a fixed uncertainty in the numerator (the uncertainty in κ_m caused by intrinsic galaxy ellipticities) by 1 factor of the decreasing quantity $1/\Sigma_{\rm crit}$; hence, the uncertainty in the quotient, the mass-to-light ratio, increases with redshift. One could reduce the uncertainty in mass-to-light ratio at larger redshifts if one had deeper catalogs, i.e., catalogs containing source galaxies at higher redshift. Thus, one should not interpret Figures 10–15, 18, and 19 as implying that there is negligible mass at redshift $z \geq 0.8$ but, rather, that without deeper catalogs one should not expect to be able to detect it.

The value of M/L_B ($\simeq 300\ h\ M_\odot/L_\odot$) obtained for the two lower redshift slices ($z = 0.2$ and $z = 0.5$) was higher than that obtained for the combined sample. We interpret a depressed M/L_B value for the combined sample as a dilution effect caused by the inclusion of high redshift ($z = 0.6$–0.9) early-type galaxies whose luminosity contributes to the autocorrelation (denominator) of equation (11) but whose mass does not contribute to the numerator because of the reasons discussed in the previous paragraph.

The M/L_B value of $\simeq 300\ h\ M_\odot/L_\odot$ obtained from the two lower redshift slices is therefore most likely to be representative for this cosmology, and this is the value we shall adopt for the remainder of the paper.

4. DISCUSSION

In the previous sections we used our CFHT data to cleanly select a sample of bright early-type galaxies using $V-I$ colors and I magnitudes and assign reasonably precise redshifts to them. We showed that there was a strong correlation between the actual mass inferred from weak lensing analysis and the mass predicted, assuming the light associated with early-type galaxies traces mass with a constant mass-to-light ratio.

This is a surprising result that was first noticed for the ms0302 supercluster by KWLK, as discussed in § 1. The caveat, in that case, of course, was that, as with all examples of *cluster* measurements, there was a strong possibility of bias and no guarantee that a cluster M/L ratio was representative of the universe in general. There may have been something unusual about the way that galaxies formed in such extremely overdense environments as clusters which was not reproduced elsewhere under more "normal" conditions of formation. In this paper we have demonstrated the remarkable result that early-type galaxy light traces mass with a constant M/L ratio appears to be a universally applicable relationship.

4.1. M/L_B in an Einstein–de Sitter Universe

The actual value of the constant of proportionality between mass and light is dependent on cosmology. We performed our analysis assuming a flat lambda ($\Omega_{m0} = 0.3$, $\Omega_{\lambda 0} = 0.7$) cosmology. We also repeated the analysis for an Einstein–de Sitter ($\Omega_{m0} = 1.0$, $\Omega_{\lambda 0} = 0.0$) cosmology. The required M/L_B ratio *increases* if this cosmology is assumed. Values of M/L_B at zero lag are shown in Table 4. The dependence of M/L_B on cosmology can be understood qualitatively from the following argument. From (4) it is clear that the predicted κ-from-light is a function of $1/\Sigma_{\rm crit}$. From Figure 9 it is clear that for an Einstein–de Sitter cosmology, $1/\Sigma_{\rm crit}$, is smaller than for the flat lambda case at all redshifts. Thus, the predicted κ-from-light in this cosmology is smaller by the same scaling factor. Note that the scaling factor is not constant but is a function of redshift, being the ratio of the height of the solid to dot-dashed line at each redshift. Hence, for this cosmology, in order to match the same κ fluctuations obtained from the κ-from-shear analysis, a *higher* value of M/L_B ratio is required.

4.2. *Comparison with other Galaxy Groups/Cluster Studies*

M/L ratios have been measured on galaxy group and cluster scales by several other teams. On group scales, Hoekstra, Franx, & Kuijken (1999) recently found an average $M/L_B = 372 \pm 122$ for galaxy groups after making a correction for luminosity evolution. On larger scales, Mellier (1999, Table 1 and references therein) summarize all published M/L ratios obtained for clusters using gravitational lensing as of 1999. One should be cautious because the different teams used different telescopes, software packages, and mass reconstruction techniques and obtained data under varying seeing and to varying physical radii from the cluster center. In addition, some teams choose to quote M/L_V in preference to M/L_B. Nevertheless, on scales of about 1 Mpc, the geometry of each cluster mass distribution inferred from gravitational lensing was similar to the galaxy distribution and also to the X-ray distribution when it was available. The M/L ratios obtained by different teams are fairly scattered but have a median value of 300, with a trend to increase with radius. As clusters contain a high fraction of elliptical galaxies, it is not so unexpected that M/L ratios for clusters turn out to be so similar to the value we derive in this paper.

4.3. *Inferred Mass Density* Ω_{m0}

We now calculate Ω_{m0}, the fractional contribution of early-type galaxy mass density to the critical mass density (where $\rho_{\rm crit} = 2.77 \times 10^{11}\, h^2\, M_\odot\ {\rm Mpc}^{-3}$),

$$\Omega_{m0} = \rho_E/\rho_{\rm crit}\ , \tag{12}$$

$$\rho_E = (M/L)_E\, \mathscr{L}_E = (M/L)_E\, \phi_{*E}\, L_{*E}\, \Gamma(\alpha_E + 2)\ , \tag{13}$$

where $\mathscr{L}_E$ is the measured B-band early-type luminosity density of the universe for *early*-type galaxies. With ϕ_{*E} of $9 \times 10^{-3} (h^{-1}\ {\rm Mpc})^{-3}$, L_{*E} of -19.61, and α_E of -0.74 (from Folkes et al. 1999), we obtain $\mathscr{L}_E = 8.83 \times 10^7\, h\, L_\odot\ {\rm Mpc}^{-3}$.

Using our M/L_B estimates for early types, and assuming an M/L ratio of $300\, h\, M_\odot/L_\odot$ (400 for Einstein–de Sitter) and an uncertainty of $\pm 25\%$ (the uncertainty in our M/L_B value is a much greater contribution to the error budget than the uncertainty from Folkes et al.), we obtain $\Omega_{m0} \simeq 0.10 \pm 0.02$ of closure density ($\Omega_{m0} \simeq 0.13 \pm 0.03$ for Einstein–de Sitter).

The global density parameter we obtain appears low compared with other estimates (Carlberg et al. 1997; Mellier 1999). This is not because our early-type M/L_B value is low but because we do not assign the same M/L_B to late-type galaxies as to early types. In the scenario we propose, late types are assumed to have very similar luminosities as early types (e.g., Folkes et al. 1999 find B_* for late types to be very similar to B_* for early types). The difference is that late types have much less mass associated with them; hence, their M/L_B ratio is much lower. The analysis in this paper assumes that they have negligible M/L_B compared to that of early types.

Interestingly, we note that the current best limit on the baryon fraction determined from Big Bang nucleosynthesis measurements, assuming $H_0 = 65\ {\rm km\ s^{-1}\ Mpc^{-1}}$, is $\Omega_B = 0.045 \pm 0.0028$ ($\Omega_B h^2 = 0.019 \pm 0.0012$ from Burles et al. 2000). From (4) and Figure 9, one would expect the M/L_B ratio for an open baryon ($\Omega_{m0} = 0.05$) universe $\simeq 350\ h\ M_\odot/L_\odot \pm 25\%$, intermediate between the flat lambda and Einstein–de Sitter values. The lower limit to the mass fraction is thus rather close to the baryon-only fraction, suggesting that baryons might be the sole source of mass in the universe. A flat lambda cosmology with $\Omega_{m0} = 0.05$ in baryons would require an M/L_B ratio *smaller* than that found for our fiducial $\Omega_{m0} = 0.3$ case, which would, in turn, *decrease* the estimates of $\Omega_{m0} \sim 0.10 \pm 0.02$ found above. We also note in passing that preliminary analyses of recent cosmic microwave background (CMB) measurements (Jaffe et al. 2000) prefer a higher value for $\Omega_B = 0.076 \pm 0.012$ ($\Omega_B h^2 = 0.032 \pm 0.005$) than that derived by Burles et al. Of course, the upper limit we obtain for the mass fraction is triple the baryon-only fraction and would require sizeable quantities of exotic matter. Additionally, other measurements, in particular supernovae constraints, suggest the universe may contain quantities of exotic matter. Note also that all mass reconstructions from weak lensing analyses are blind to any uniform density component, so, in actuality, our M/L_B ratios should be considered to be lower limits.

4.4. *Possible Uncertainties*

As a consistency check, we repeated the mass-luminosity correlation analysis in § 3 but for I- and V-band catalogs separately. We obtained similar values of significance and M/L_B (within our 25% uncertainties) as a function of redshift as had been obtained for the best composite catalog.

The value of M/L_B we infer is strongly dependent on both cosmology and source redshift distribution. Although we believe the effect of any uncertainty in the redshift distribution of the source galaxies is largely dwarfed by intrinsic galaxy shape and measurement errors, we note that if the redshift distribution were in error and source galaxies were in fact at higher (lower) redshift than our estimate, the inferred M/L_B ratio would decrease (increase).

In addition, if there were some evolution in L_* such that galaxies were brighter by a few tenths of a magnitude between $z = 0.5$ and the present, this would force an upward revision to the M/L_B ratio inferred for the $z = 0.5 \pm 0.15$ sample. That the $z = 0.2 \pm 0.15$ and $z = 0.5 \pm 0.15$ M/L_B values are so similar (Table 4) argues against strong luminosity evolution in the early-type galaxies between redshift 0.5 and the present.

In the analysis performed in this paper, we were forced by the availability of only two passbands to select early-type galaxies within 1–2 mag of L_*. Presumably, M/L_B might not be constant with decreasing luminosity. However, the M/L_B ratio cannot increase dramatically at the faint end of the luminosity function; i.e., faint galaxies cannot be very massive relative to their luminosity or the correlation between mass and bright early-type light seen in Figure 16 would not be so convincing. Also, there is, of course, some mass associated with late-type galaxies. Any mass associated with late-type galaxies will contribute to the noise in Figures 16 and 19. However, as mentioned in § 3.4, it cannot be dominant compared with that of the early types or, again, we would not see such a strong mass–to–early-type–luminosity correlation.

Note that the values of M/L_B derived in this paper are entirely consistent with M/L_B ratios for galaxy halos derived in Paper II from a galaxy-galaxy lensing analysis. In that paper, we found a typical mass-to-light ratio of $M/L_B \simeq 121 \pm 28\ h\ (r/100\ h^{-1}\ \mathrm{kpc})$ (for L_* galaxies). In this paper, we found that halos extend to $\simeq 2'$ at $z \sim 0.2$ (Fig. 18), which corresponds to $r \sim 280\ h^{-1}$ kpc. Within that radius, we therefore predict a M/L_B of $2.8 \times 121 \pm 28\ h\ M_\odot/L_\odot = 340 \pm 80\ h\ M_\odot/L_\odot$ from that paper [assuming a flat lambda ($\Omega_{m0} = 0.3$, $\Omega_{\lambda 0} = 0.7$) cosmology], which compares well with the M/L_B of $300 \pm 75\ h\ M_\odot/L_\odot$ derived from this paper.

We note that in Paper II we adopted a different relationship between galaxy mass and light. On small scales ($\lesssim 10\ h^{-1}$ kpc), it has been shown empirically that mass is approximately proportional to the square root of luminosity of early-type galaxies, i.e., $M \propto \sqrt{L}$ (Faber & Jackson 1976; Fukugita & Turner 1991). In this paper, we are probing scales larger than individual galaxy halos, and it seems more reasonable to assume $M \propto L$ on these scales. Incidentally, the $M \propto \sqrt{L}$ relationship on small scales also justifies our choice of smoothing scale ($45'' \sim 200\ h^{-1}$ kpc at $z = 0.5$). A smoothing scale of a few hundred h^{-1} kpc ensures we are investigating scales "one step up" from individual galaxy halos where M/L biases on very small scales would tend to average out.

On the basis of the data set described in this paper, it would be premature to claim definitively that (early-type galaxy) luminosity traces mass with a *constant* mass-to-light ratio. The luminosity-luminosity and mass-luminosity profiles do appear remarkably similar. However, the uncertainties are sizeable ($\simeq 25\%$). We conclude that there is no evidence for (early-type galaxy) luminosity and mass segregation on galaxy group and cluster scales but that larger quantities of data will be required to determine empirically the mass-to-luminosity dependence to greater precision. That mass should be directly proportional to luminosity is a very appealing relationship, but nature may have conspired otherwise, and there may well still be scope for some amount of biased galaxy formation.

5. CONCLUSIONS

Using $V-I$ color and I magnitude, we cleanly selected bright early-type galaxies. We measured the gravitational shear from faint galaxies and found a strong correlation with that predicted from the early-type galaxies if they trace the mass with $M/L_B \simeq 300 \pm 75\ h\ M_\odot/L_\odot$ for a flat ($\Omega_{m0} = 0.3$, $\Omega_{\lambda 0} = 0.7$) lambda cosmology and $M/L_B \simeq 400 \pm 100\ h\ M_\odot/L_\odot$ for Einstein–de Sitter. We made two-dimensional reconstructions of the mass surface density. Cross-correlation of the measured mass surface density with that predicted from the early-type galaxy distribution showed a strong peak at zero lag. We azimuthally averaged the cross- and autocorrelation functions. We concluded that the profiles were consistent with early-type galaxies tracing mass on scales of $\geq 45''$ (the smoothing scale). We subdivided our bright early-type galaxies by redshift and obtained similar conclusions. These M/L_B ratios imply $\Omega_{m0} \simeq 0.10 \pm 0.02$ ($\Omega_{m0} \simeq 0.13 \pm 0.03$ for Einstein–de Sitter) of closure density.

In summary, we found that the majority of mass in the universe is associated with early-type galaxies. On scales of $\geq 200\ h^{-1}$ kpc, it appears that their light traces the underlying mass distribution with a constant $M/L_B = 300$–$400 \pm 100\ h\ M_\odot/L_\odot$, depending on cosmology. As with several other recent results, our data argues against an $\Omega_{m0} = 1$ universe.

In the future it will be possible to measure M/L_B ratios more precisely. The total areal coverage in this paper was 1.5 deg^2. Future planned surveys such as the Hawaii Lensing Survey, the Deep Lens Survey, or the Megacam/Terapix consortium will cover a much larger area and, hence, reduce uncertainties in M/L_B. In addition, more precise constraints on cosmology (Ω_{m0} and $\Omega_{\lambda 0}$) should soon be available from CMB measurements, supernovae, and the deep lensing surveys themselves. The color-redshift degeneracy could be broken by an increased number of passbands to provide photometric redshifts. The greater range of absolute luminosity then available (limited here to $L \sim L_* \pm 1$–2) would allow mass-to-luminosity dependence (assumed in this work to be $M \propto L$) to be determined more precisely, both as a function of luminosity and as a function of distance from galaxy center. Finally, the availability of greater than two-passband data will also allow photometric redshifts to be determined for late-type galaxies and a similar investigation to be undertaken into their M/L ratios.

We thank Douglas Burke and Len Cowie for many useful discussions. We also thank Marc Davis, the referee, for his constructive comments. G. W. gratefully acknowledges financial support from the estate of Beatrice Watson Parrent and from Mr. and Mrs. Frank W. Hustace, Jr., while Parrent Fellow at the University of Hawaii. This work was supported by NSF grant AST 99-70805.

REFERENCES

Bahcall, J. N., & Tremaine, S. 1981, ApJ, 244, 805
Bahcall, N. A., Lubin, L. M., & Dorman, V. 1995, ApJ, 447, L81 (BLD)
Bardeen, J. M., Bond, J. R., Kaiser, N., & Szalay, A. S. 1986, ApJ, 304, 15
Bosma, A. 1981, AJ, 86, 1825
Branchini, E., Zehavi, I., Plionis, M., & Dekel, A. 2000, MNRAS, 313, 491
Brown, M. E., & Peebles, P. J. E. 1987, ApJ, 317, 588
Burles, S., Nollett, K. M., Truran, J. M., & Turner, M. S. 2000, ApJ, 552, L1
Carlberg, R. G., Yee, H. K. C., & Ellingson, E. 1997, ApJ, 478, 462
Carlberg, R. G., Yee, H. K. C., Ellingson, E., Abraham, R., Gravel, P., Morris, S., & Pritchet, C. J. 1996, ApJ, 462, 32
Cowie, L. L., Gardner, J. P., Hu, E. M., Songaila, A., Hodapp, K. W., & Wainscoat, R. J. 1994, ApJ, 434, 114
Cowie, L. L., Songaila, A., & Barger, A. J. 1999, AJ, 118, 603
Cowie, L. L., Songaila, A., Hu, E. M., & Cohen, J. G. 1996, AJ, 112, 839
Davis, M., Efstathiou, G., Frenk, C. S., & White, S. D. M. 1985, ApJ, 292, 371
Davis, M., & Geller, M. J. 1976, ApJ, 208, 13
Davis, M., Miller, A., & White, S. D. M. 1997, ApJ, 490, 63
Davis, M., & Peebles, P. J. E. 1983, ApJ, 267, 465
Faber, S. M., & Gallagher, J. S. 1979, ARA&A, 17, 135
Faber, S. M., & Jackson, R. E. 1976, ApJ, 204, 668
Folkes, S., et al. 1999, MNRAS, 308, 459
Fukugita, M., & Turner, E. L. 1991, MNRAS, 253, 99
Hoekstra, H., Franx, M., & Kuijken, K. 2001, in ASP Conf. Ser. 237, Gravitational Lensing: Recent Progress and Future Goals, ed. T. Brainerd & C. Kochanek (San Francisco: ASP), in press
Jaffe, A., et al. 2000, Phys. Rev. Lett., 86, 3475
Jing, Y. P., Mo, H. J., & Boerner, G. 1998, ApJ, 494, 1
Kaiser, N. 1984, ApJ, 284, L9
———. 2000, ApJ, 537, 555
Kaiser, N., & Squires, G. 1993, ApJ, 404, 441
Kaiser, N., Wilson, G., & Luppino, G. 2001a, preprint (astro-ph/0003338) (Paper I)
Kaiser, N., Wilson, G., Luppino, G., & Dahle, H. 2001b, preprint (astro-ph/9907229)
Kaiser, N., Wilson, G., Luppino, G., Kofman, L., Gioia, I., Metzger, M., & Dahle, H. 2001c, preprint (astro-ph/9809268) (KWLK)
Kim, D., & Fabbiano, G. 1995, ApJ, 441, 182
Mellier, Y. 1999, ARA&A, 37, 127
Mushotzky, R. F., Loewenstein, M., Awaki, H., Makishima, K., Matsushita, K., & Matsumoto, H. 1994, ApJ, 436, L79
Sandage, A. 1986, ApJ, 307, 1
Shaya, E. J., Peebles, P. J. E., & Tully, R. B. 1995, ApJ, 454, 15
Sigad, Y., Eldar, A., Dekel, A., Strauss, M. A., & Yahil, A. 1998, ApJ, 495, 516
Strauss, M. A., & Willick, J. A. 1995, Phys. Rep., 261, 271
Trimble, V. 1987, ARA&A, 25, 425
Trinchieri, G., Fabbiano, G., & Kim, D. 1997, A&A, 318, 361
Trinchieri, G., Kim, D., Fabbiano, G., & Canizares, C. R. C. 1994, ApJ, 428, 555
Turner, E. L. 1976, ApJ, 208, 304
White, D. A., & Fabian, A. C. 1995, MNRAS, 273, 72
Willick, J. A., & Strauss, M. A. 1998, ApJ, 507, 64
Wilson, G., Kaiser, N., Luppino, G., & Cowie, L. L. 2001, ApJ, 555, 572 (Paper II)
Wittman, D. M., Tyson, J. A., Kirkman, D., Dell'Antonio, I., & Bernstein, G. 2000, Nature, 405, 143
Zaritsky, D., Smith, R., Frenk, C., & White, S. D. M. 1997, ApJ, 478, 39
Zwicky, F. 1933, Helvetica Phys. Acta, 6, 110